X-Ray Photoelectron Diffraction Studies of the Micas Lepidolite and Biotite†‡

Lynne A. Ash, (in part) Stephanie L. Clark, Stephen Evans,* and Anthony G. Hiorns
Edward Davies Chemical Laboratories, University College of Wales, Aberystwyth, Dyfed SY23 1NE

Comprehensive *X*-ray photoelectron diffraction (x.p.d.) data for a Norwegian 1M lepidolite and a 1M biotite are reported and discussed. Improved techniques for the collection and processing of x.p.d. patterns are described, including a new procedure for correcting for the variation of instrumental response with the electron take-off angle. Comparison of x.p.d. patterns from rotation about near-equivalent axes at 120° to each other reveals that two major features in the interlayer ion patterns cannot be attributed to scattering by atoms nearer than 10—13 Å from the emitting site. Enhanced anisotropy in the Rb 3*d* patterns relative to those for K 2*p* is discussed. It is shown that x.p.d. experiments involving polar rotations about an axis parallel to the unit-cell vector *a* can be used to detect octahedral cation ordering involving differentiation of the two sites with *cis*-OH groups; a similar method for detecting tetrahedral cation ordering is suggested. Rotation about axes at 120° to *a* is valuable for the identification of elements segregating equally into the two *cis* octahedral sites, while experiments involving rotation about axes parallel to and at 120° to the unit-cell vector *b* enable octahedral cation ordering amongst all three octahedral sites to be characterised. By these means octahedral Li and Mn in the lepidolite are shown to be concentrated in the *trans* M(1) site, and Al in M(3) (one of the two *cis* sites equivalent in *C*2/*m* symmetry). This mica thus has only *C*2 symmetry. The 1.2% of Ti in the biotite is segregated uniformly into the two *cis* octahedral sites, unlike the Mg and Fe which are distributed randomly amongst all three octahedral sites. Tetrahedral ordering was not detected in either mica.

X-Ray photoelectron diffraction (x.p.d.), first described some 17 years ago,[1] has in recent years been exploited, with the aid of single-scattering cluster calculations, to characterise many adsorbate structures;[2] it is now a rival to low-energy electron diffraction (l.e.e.d.) for the determination of surface structure. In parallel with these developments, it was realised, while developing methods of quantifying the *X*-ray photoelectron spectra of aluminosilicates,[3] that, because of the differences in local environment, atoms occupying different sites *within* a single crystal gave rise to different anisotropies in photoelectron emission which could yield structural information about isomorphous substitution even at low concentrations.[4] The micas are ideal for this type of study, being readily available as large single crystals, easily cleaved to yield clean surfaces, and chemically unreactive, but other materials for which analogous information is valuable, such as the spinels,[5] can also be studied.

In this paper we describe first the semi-automated methods which have superseded our earlier, more primitive, data-collection procedures. The results of a comprehensive investigation, facilitated by these techniques, of x.p.d. in two of the micas previously studied, a lepidolite from Høydaler, Telemark, Norway[6] and a biotite from an unknown location[7,8] are then presented and discussed.

Compensation for the variation of the instrumental response with the electron take-off angle (or polar angle), θ, was not formerly possible, and results were thus necessarily reported in the form of graphs showing normalised ratios between *X*-ray photoelectron spectroscopy (x.p.s.) peak intensities as a function of θ. Such plots are independent of the response function.[9] A correction procedure for the response function has now been developed, and we report for the first time the angular dependence of both ratios and individual peak intensities. The former remains the most easily interpreted format for some applications,[10] and can often be determined with greater precision than the angular dependence of the intensity for an individual peak, but the physical origin of the anisotropy is more readily appreciated in the latter format.

A principal aim of the present work was to examine the tentative suggestion[6] that differences between the Al and Mn, Li patterns in the lepidolite were due to octahedral cation ordering and to investigate whether differences between the Ti and Mg,Fe patterns in the biotite[7] could also be explained in this way. One approach to this task would be to develop a quantitative theoretical model within which the x.p.d. patterns could be calculated. Progress is being made[11] in this but results for solids as complex as the micas are not yet practicable. The alternative adopted here is to collect a comprehensive set of x.p.d. patterns for both micas (the previous data related to rotation about only one axis) and apply qualitative arguments, largely based on symmetry, to the resulting data. In addition to providing more definitive evidence relating to cation ordering in these micas, an improved understanding of the x.p.d. phenomenon itself was also anticipated.

The Physical Origin of X-*Ray Photoelectron Diffraction*.—Because of the electron wavelengths (λ = *ca.* 0.3 Å) and angles involved, the positions of x.p.d. peaks on the angular scale cannot be predicted by application of Bragg's law. These positions can, however, for simple crystals, be correlated directly with densely packed planes within the crystal, the Bragg angles then being related to the *widths* of the peaks. In this 'electron channelling' or 'Kikuchi band' description,[12] the angular anisotropy is thus associated with structural features of an (implicitly infinite) crystal. Recently, however, x.p.d. experiments on nickel single crystals before and after deposition of epitaxial overlayers of Cu[13] have shown that the x.p.d. effect can be convincingly described in terms of enhanced forward elastic scattering of the outgoing photoelectron wave by atoms near to the emitting site. These experiments suggest that x.p.d. effects are relatively short-range, scatterers beyond *ca.* 9 Å

---

† Presented at a meeting of the Polar Solids Discussion Group of the Royal Society of Chemistry, 15th December, 1986.

‡ *Non-S.I. units employed:* eV ≈ 1.60×10^{-19} J; Torr ≈ 133 Pa.

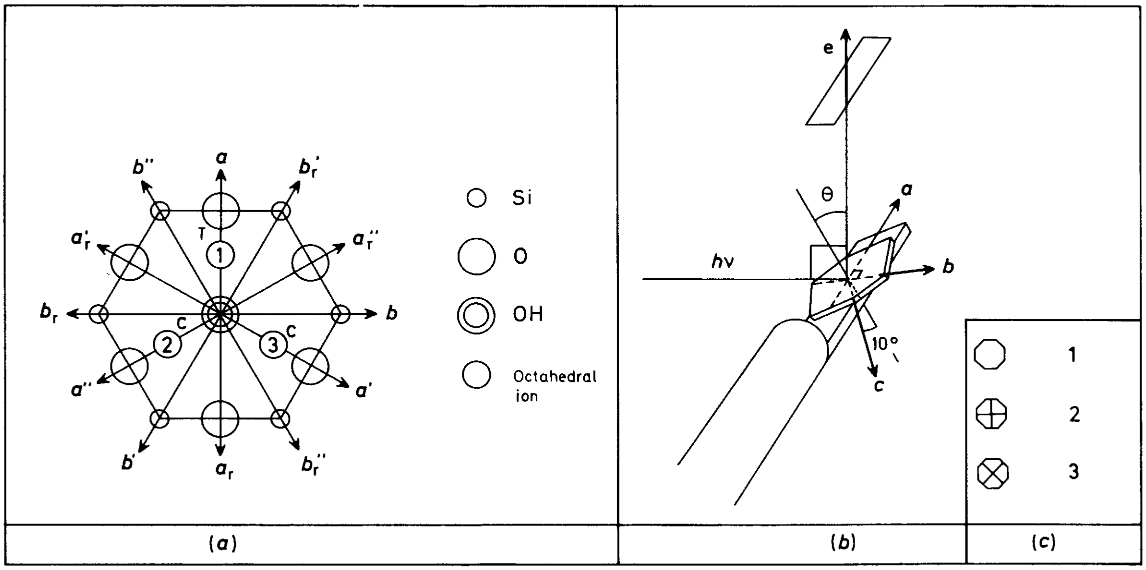

Figure 1. (*a*) Axes of rotation in relation to the mica structure: the *c* axis is directed into the plane of the paper. T and C indicate an octahedral ion with *trans* and *cis* OH,F groups respectively. The *cis* sites labelled 2 and 3 are equivalent in $C2/m$ symmetry. (*b*) Axes of rotation in relation to the experimental geometry. e Represents the electron beam detected by the analyser. The analyser entrance slit is located vertically above the sample; *a*, *b*, and *c* represent the unit-cell vectors of the mica. The crystal is shown in the orientation denoted by *a*, *i.e.* the *a* vector lies parallel to the axis of rotation of the probe. The angle between the incident *X*-rays and the detected electron beam is constant at *ca.* 90°. (*c*) Symbols applicable to Figures 3—15

having only a small influence on the anisotropy of electron emission. The electron attenuation length in mica, however, is *ca.* 34 Å at 1 144 eV,[4] rather longer than in typical metals (*ca.* 14 Å[14]), and so longer range effects may be more significant in the micas. The 'enhanced-forward-scattering' concept, unlike the Kikuchi-band approach, allows a distinction easily to be made between different emitting sites in a complex crystal, and both approaches have qualitative utility in appropriate circumstances.

The angular anisotropy is fundamentally related to deviations from plane-wave character of the final state of the photoelectron, resulting from the presence of neighbouring atoms.[11] Such a description emphasises the close relationship between x.p.d. and EXAFS (extended *X*-ray absorption fine structure), another new technique for solid-state structure determination,[15] and is the starting point for the development of a quantitative theory.[16]

The Structures and Compositions of the Micas.—Each layer in an ideal mica structure is built up from upper and lower sheets, each consisting of MO_4 tetrahedra linked by their corners into approximately hexagonal rings, enclosing a central sheet of octahedrally co-ordinated cations, which share oxide ions with the tetrahedral sheets.[17,18] The co-ordination shell of the octahedral cations is completed by OH^- and F^- anions: two thirds of the cations [usually designated as M(2)] have a pair of *cis* OH,F neighbours and the remainder [M(1)], *trans* OH,F groups. The layer is characterised by a C_2 rotation axis and a mirror plane; the *a* unit-cell vector (5.3 Å) lies in this plane, perpendicular to the C_2 axis, *b* (9.2 Å) lies parallel to this axis, and the planes containing both *a* and *b* lie parallel to the cleavage planes. At 120° to both *a* and *b* directions, 'pseudo-*a*' and 'pseudo-*b*' directions can be identified. The similarity of environment for atoms in corresponding positions is however limited to neighbours within a few Å perpendicular to the layers because of the $-a/3$ offset between the upper and lower tetrahedral sheets in each layer, necessary to accommodate the inclined octahedra in the central sheet. The distance traversed before non-equivalence is first encountered increases progressively as the direction sampled approaches a plane parallel to the layer. We show below that both the micas studied here are 1M polytypes, in which the $a/3$ offset occurs in the same direction in every layer. The mirror plane then ideally extends throughout the crystal, which has $C2/m$ symmetry.

In our x.p.d. experiments, a range of *ca.* 90° in θ ($-10 < \theta < 80°$, specified throughout with respect to the normal to the surface) is the maximum practicable, whereas conceptually a range of 180° exists for each rotation axis. Rotation of the sample through 180° azimuthally, followed by repetition of the experiment through the same range of θ, permits *ca.* 160° to be investigated experimentally. For $\theta > 80°$ electron refraction within the crystal becomes significant and ultimately internal electron reflection prevents examination of the last few degrees.[9] Throughout, we shall denote directions along axes parallel to *a* and *b* and their associated x.p.d. patterns by *a*, a_r, and b,b_r, the subscript r denoting 'reversal' (180° azimuthal rotation) of the crystal. Experimental axes of rotation parallel to the pseudo-*a* and -*b* vectors and their associated patterns are then designated a', a'_r, a'', a''_r and b', b'_r, b'', and b''_r. All have been investigated experimentally for both micas. The experimental axes of rotation are related to the crystal structure in Figure 1(*a*) and (*b*); the directions of *a* and a_r were established by Laue photography as described in the next section. Figure 1(*c*) shows the symbols used in later figures.

The near-surface regions of these micas have compositions close to the rational formulae[6,7] $(K_{0.81}Rb_{0.11})(Li_{1.50}Al_{1.19}Mn^{II}_{0.31})(Si_{3.39}Al_{0.61})O_{10}(OH)_{0.4}F_{1.6}$ (lepidolite) and $(K_{0.85}Na_{0.02})(Fe^{II}_{1.24}Mg_{0.99}Al_{0.46}Ti_{0.11}Li_{0.02})(Si_{2.93}Al_{1.07})O_{10}(OH)_{1.6}F_{0.4}$ (biotite).

Experimental

Determination of the Polytype and Orientation of the Micas.—The *c* repeat distances, which are *ca.* 10 Å for the 1M micas, 20 Å for the $2M_1$ and $2M_2$, and *ca.* 30 Å for a 3T mica,[18] were determined from oscillation photographs of small samples of each mica. Initially, mechanical cutting or sawing caused so much damage to the edges of the flake that very indistinct photographs were obtained. Larger crystals (2—3 mm) were therefore cut, and suspended briefly in molten NaOH: the damaged regions were thereby dissolved, and after washing with dilute HCl and water the (now much smaller) crystals were mounted in the usual way. For the biotite, all the specimens so examined had a single-layer repeat. The lepidolite crystals actually studied by x.p.d. also had a one-layer repeat, but three-layer (3T) and 20-Å crystals were also found.

It is necessary also to demonstrate the presence of a mirror plane in a one-layer structure to identify the polytype as 1M, because disordered stacking of the layers is not uncommon.[17,18] A close approximation to a mirror plane was easily located in transmission Laue photographs of both micas (camera-to-sample distance 2.5 cm), and tilting the crystals so that the *c* direction lay parallel to the *X*-ray beam then enabled the *a* and *b* directions to be identified both on the crystals previously studied by x.p.d. and on those studied here. Laue photographs were taken at 2—4 mm intervals over the entire surface of the lepidolite crystals after x.p.d. study, to confirm their structural homogeneity. Small regions of 3T and 2M structures were found near one edge, but because of their small size and position near the crystal periphery they are most unlikely[19] to have affected the x.p.d. data significantly.

A number of Laue photographs were also taken from different portions of the original large crystal of biotite: the mirror plane was always present and in the same orientation even for samples taken as much as 20 cm laterally and several mm vertically from each other. The layer orientation is thus preserved over very long distances.

Collection of X.P.D. Data.—The mica samples were cut from cleaved flakes < 1 mm thick to hexagonal shapes about 10 mm across. In the lepidolite (as with other micas we have studied) a clearly visible striation (a slight ridge) observed at the edge of the x.p.d. crystal was found to be accurately aligned parallel to *b*; for the biotite one edge of the crystal was cut as accurately parallel to *b* as possible (*ca.* 1°). The crystals were mounted by stainless-steel screws and clips, coated with Aquadag colloidal graphite to ensure that no peaks other than C 1*s* could originate from the mountings. Alignment of the rotation axis was achieved visually using a protractor in conjunction with the above-mentioned striation (lepidolite) or the crystal edge (biotite).

Each data set comprised *ca.* 24 groups of *X*-ray (Mg-K_α) photoelectron spectra, recorded at 3.75° intervals in θ using an AEI/Kratos ES200A electron spectrometer with a multichannel analyser (MCA) and microcomputer data system.[20] This angular interval is comparable with the instrumental angular resolution: diagrams of the electron emission geometry have been given elsewhere.[19,21] The data were collected in 0.25-eV channels during multiple sweeps at 0.5 eV s^{-1} and acccumulated in the MCA: considerably more sweeps were required for the weaker peaks to secure acceptable signal-to-noise ratios. Typical automated data collection sequences are shown in Table 1. Each group of spectra required *ca.* 60 min to collect; any (small) time-dependent drift in overall sensitivity was, by such sequencing, largely averaged out.

Adventitious carbon contamination was removed (usually daily) from the lepidolite crystals by exposure to microwave-excited nitric oxide (a potent source of active oxygen[22]), at *ca.* 70 °C for < 300 s at *ca.* 5 × 10^{-5} Torr, in the sample preparation chamber of the spectrometer. This process had a negligible effect on the spectrum of the underlying mica. Small progressive changes were noted in the O 1*s* profile, well away from the peak maximum, probably arising from surface oxygen-containing groups on the Aquadag coating the sample mounting clips. The same lepidolite surface could therefore be used for all the *b*-group data (12 sets) and the first four sets of *a*-group data. However, because (as described below) the *a* and a_r patterns were found (unexpectedly) to be significantly different, a third pair of patterns was collected using a different surface cleaved from the same original crystal. Data for the four remaining axes were then collected using the latter surface.

Table 1. Data-collection sequences for the typical data shown in Figure 2(*a*)—(*d*)

Biotite	Initial kinetic energies (eV) of sections	Energy scanned per sweep (eV)
	779 1 183 528 709 944 1 086 1 120	
	* ——— * ——— * ——— * ——— * ——— * ——— * ——— *	
	←——————— 3 ———————→	174
	←—— 3 ——→	54
Sweep†	← 18 →	15
sequence	←—— 3 ——→	54
	←——————— 3 ———————→	174

Lepidolite	Initial kinetic energies (eV) of sections	Energy scanned per sweep (eV)
	1 184 597 708 945 1 087 1 120 1 168	
	* ——— * ——— * ——— * ——— * ——— * ——— * ——— *	
Sweep†	←——————— 4 ———————→	139
sequence	← 40 →	22
	←——————— 4 ———————→	139

† Number of sweeps is indicated.

The effect of oxidative cleaning on the biotite was more severe. Although no major changes were observed in the spectra, the surfaces appeared slightly 'hazy' on removal from the instrument, and after prolonged exposure stresses induced in the surface (presumably as a consequence of oxidation of octahedral Fe^{II} to Fe^{III}) caused very thin layers to curl up and cleave spontaneously from the crystal on exposure to the atmosphere. Consequently, exposure of the biotite to this cleaning process was minimised, and new surfaces were exposed by cleavage for almost every data set (*i.e.* group of 24 spectra).

Each distinct pattern was collected at least twice to establish reproducibility, so that for the lepidolite 22 complete data sets were ultimately collected. The *b*, b', and b'' data from the biotite were, however, in general, not significantly different; nor were b_r, b'_r, and b''_r. Similarly, *a* and a_r were essentially identical, as were a' and a''_r, and a'' and a'_r. Consequently 12 data sets sufficed for this mica. The total data-collection time was in excess of 1 000 h: with a more sensitive modern instrument either the sample size or the collection time could have been substantially reduced.

Duplicate data sets were never collected immediately following the initial set; the crystals were reoriented for every set. No effects persisting through both sets are thus likely to be due to random azimuthal alignment errors, which we assess as < 2°.

Data Processing.—First, the Mg-$K_{\alpha3,4}$ *X*-ray satellite peaks were subtracted[23] and the data smoothed by convolution with a Gaussian function.[24] The optimum results [assessed by the quality of the straight-line x.p.d. patterns subsequently obtained for two shells of the same element close in kinetic energy (k.e.)] were given (as expected) by using the broadest Gaussian which did not cause adjacent peaks from different elements to overlap (full width at half maximum = 2 eV).

Initially, backgrounds were subtracted using the Shirley approximation[25] except when (unusually) the background was greater to high k.e. (in which case a linear function was assumed), and peak areas obtained by numerical integration. However, although peak areas are essential for obtaining reliable elemental compositions from x.p.s., it was found that areas are not as precise an indication of *relative* intensity as are

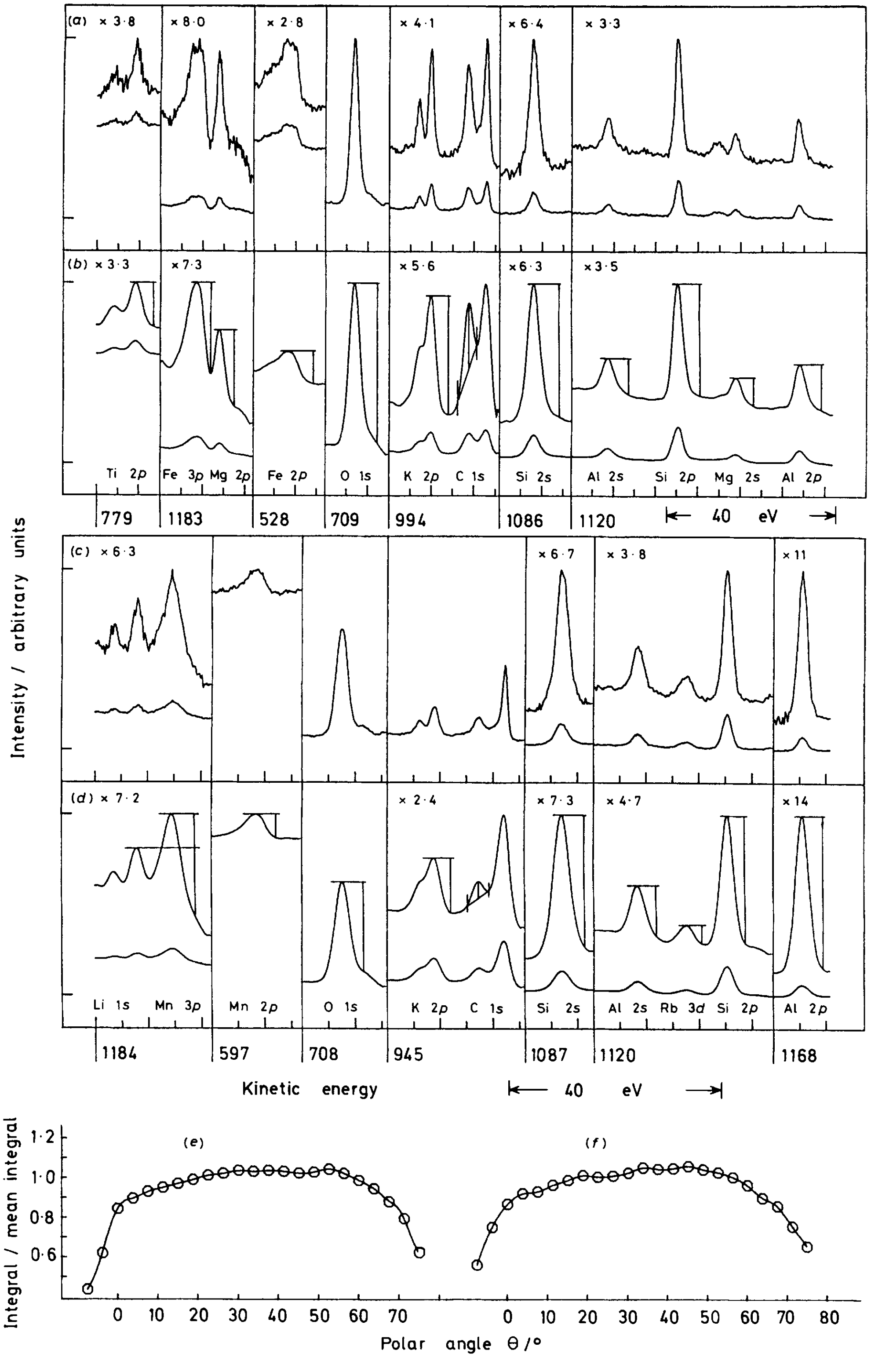

Figure 2. (*a*) Typical data for the biotite, as collected; (*b*) after removal of $K_{\alpha 3,4}$ satellites and smoothing; (*c*) and (*d*) typical data for the lepidolite, as in (*a*) and (*b*); (*e*) and (*f*) typical normalising functions for biotite and lepidolite respectively, see text

peak heights. Errors in the level of the background intensity affect areas far more than heights because peaks are broadest at the base.

Each peak maximum was therefore located between previously determined limits approximating to background to low and high k.e. by means of a least-squares quadratic fit to the highest five data points.[26] The background was then taken as the height at a preselected energy 3—6 eV to higher k.e., as before,[6,7] and the net intensity recorded as the difference between the height at the turning point of the quadratic and that

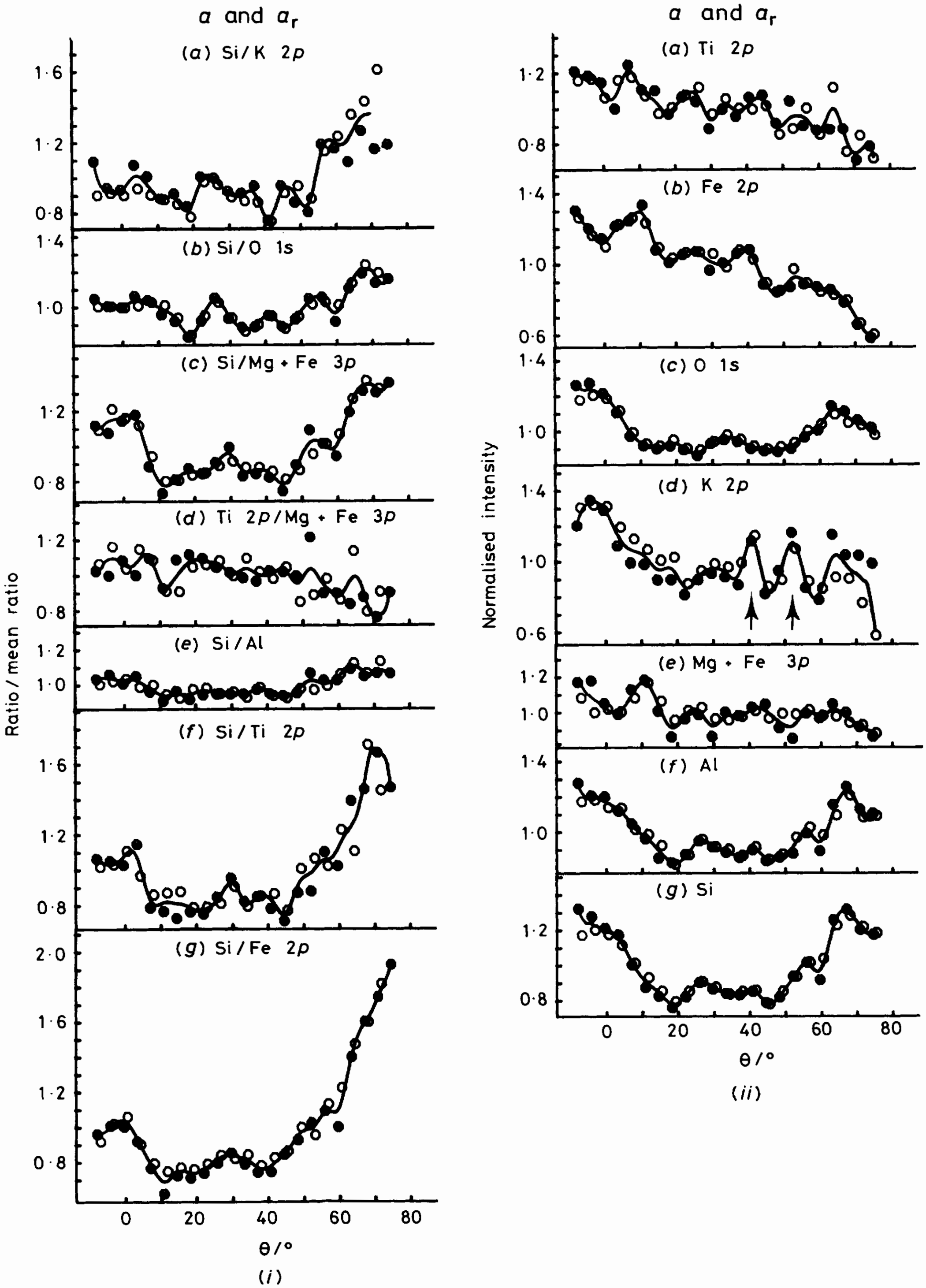

Figure 3. (*i*) Biotite x.p.d. patterns, for the a and a_r rotations. Ordinate, normalised x.p.s. peak intensity ratio; abscissa, polar angle, θ. The solid lines indicate the mean values of the normalised ratios. Mg = Mg 2*s* + Mg 2*p*; Al = Al 2*s* + Al 2*p*; Si = Si 2*s* + Si 2*p*. Symbol types 1 and 3 (see Figure 1) identify data obtained by rotation about the a and a_r axes respectively. (*ii*) x.p.d. curves corresponding with the patterns in (*i*). Ordinate, normalised peak intensities (corrected for instrumental response function); abscissa, electron take-off angle, θ. The mean values of the peak intensities are indicated by the solid lines

at the defined background energy. Linear interpolation between data points in the background region was used to keep the energy separation (peak to background) constant for each peak. The application of these processing steps, and the limits used, are illustrated in Figure 2(*a*)—(*d*).

The C 1*s* region was recorded to allow a correction for attenuation due to surface contamination. This region shows two close peaks, that at higher k.e. arising from the Aquadag on the sample mounting clips. Two sets of spectra at one value of θ were sometimes recorded, the second after standing *in vacuo* for > 15 h. These usually showed a significantly larger contaminant C 1*s* peak and lower intensities for the mica peaks. Comparison of the two allowed an attenuation factor {effectively exp[$-$(contamination layer thickness/λ cos θ)] [9]} to be estimated from

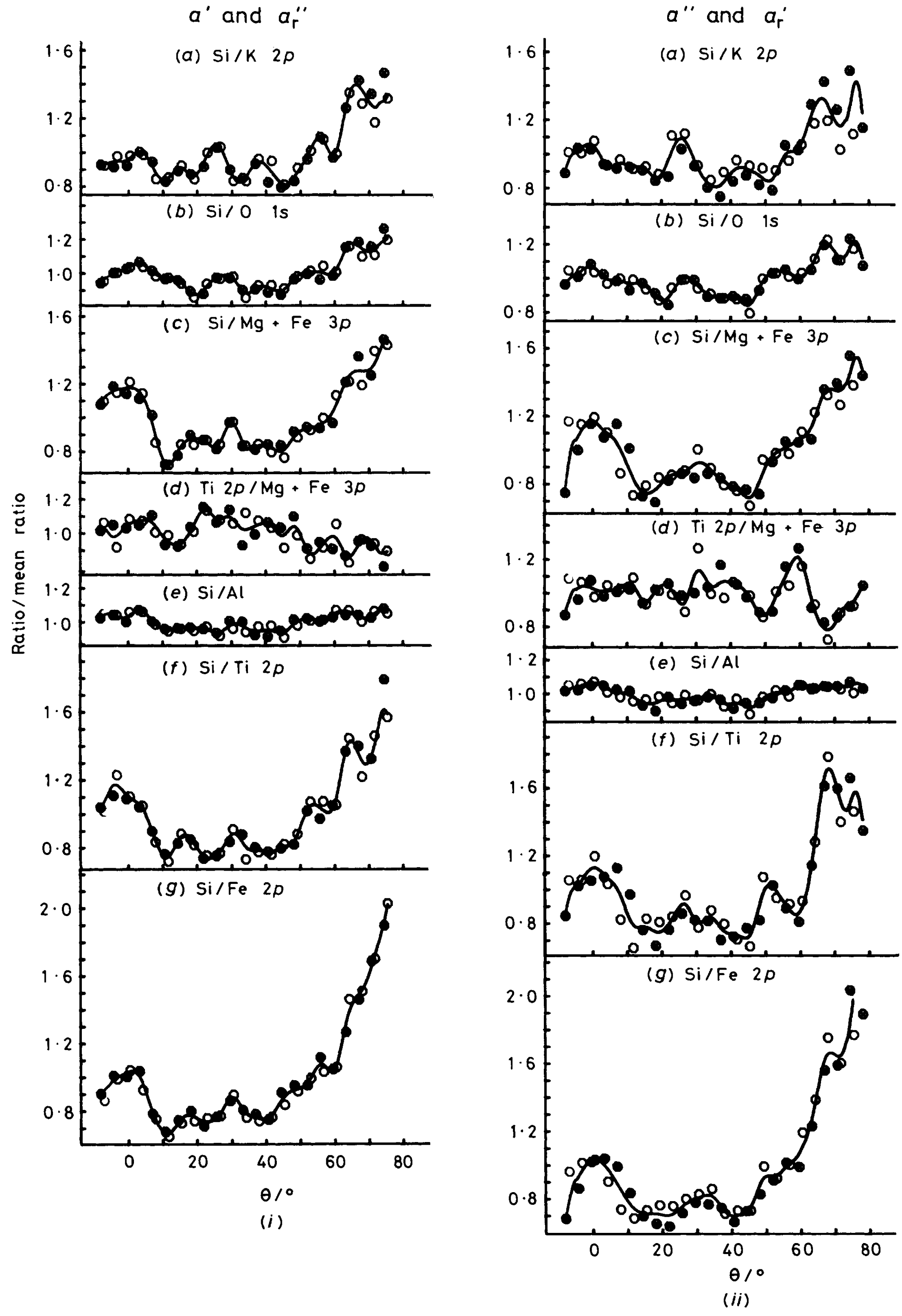

Figure 4. Biotite x.p.d. patterns for the pseudo-*a* rotations: (*i*) for the *a*′ and a_r'' rotations (symbol types 1 and 3 respectively), and (*ii*) for the *a*″ and a_r' rotations (symbol types 1 and 3 respectively)

the contaminant C 1*s* intensity for any other similar data set. These corrections were never greater than a few per cent.

X.p.d. patterns (plots of peak intensity ratio/mean ratio *vs.* θ) were then computed and plotted as before.[6,7] Since all peaks from a given site which occur close in k.e. have indistinguishable x.p.d. patterns,[4—7] Si 2*s* and Si 2*p* data were summed, as were Al 2*s* and Al 2*p*, Mg 2*s*, Mg 2*p* and Fe 3*p* (biotite) and Mn 3*p* and Li 1*s* (lepidolite). Magnesium and Fe in the biotite, and Mn and Li in the lepidolite, were previously found[6,7] to yield essentially equivalent x.p.d. patterns. These summations improved the reproducibility of the patterns significantly. Ultimately, using a mainframe computer, the x.p.d. patterns could be obtained within an hour of completion of data collection.

When plotting sets of patterns on common axes, lateral

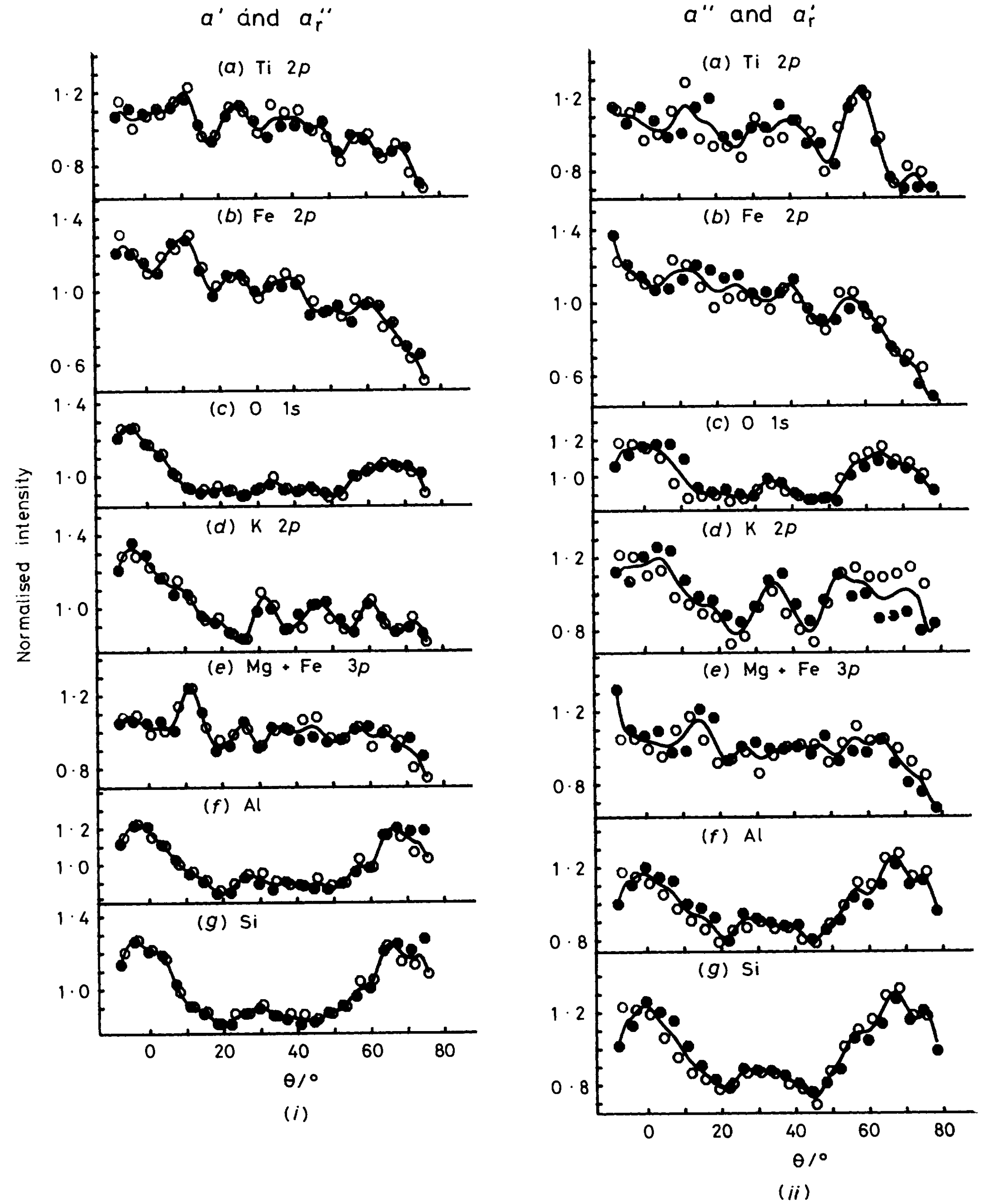

Figure 5. X.p.d. curves corresponding to the patterns of Figure 4

(angular) alignment was achieved by minimising the root-mean-square difference between the different data sets as a function of angular offset. This was necessary because the original visual alignment was less precise than the width of the sharpest features of the patterns.

Finally, the symmetry properties of the crystal were used to establish the correct absolute scale for each plot. In $C2/m$ symmetry, a pair of experiments differing only by 180° azimuthal rotation and carried out with the rotation axis parallel to a should be equivalent, whereas for a rotation axis parallel to b they correspond to rotating the crystal in opposite senses about $\theta = 0°$. For sets of a and a_r data obtained without disturbing the angular relationship between the crystal surface and the scale on the probe, the true scale was therefore obtained by dividing the angular offsets required to align the two sets of data equally between the two sets: the presence of mirror symmetry in the regions of the patterns above and below 0° confirmed the accuracy of the resultant scale. For similarly matched b-group patterns, offsets were applied so that the region of the patterns for $-10 < \theta < 10°$ in b_r coincided with $10 > \theta > -10°$ in b, again dividing the required offset equally between the two sets. Absolute scales for the remaining data were assigned by analogy. We estimate the accuracy of these scales as $\pm 1°$ in θ.

Correction of Individual Peak Intensities for the Instrumental Response Function.—Any X-ray photoelectron spectrum consists of the primary photoelectron peaks, the intensities of which are modulated by x.p.d. in single crystals, superimposed on a background of inelastically scattered photoelectrons. For a

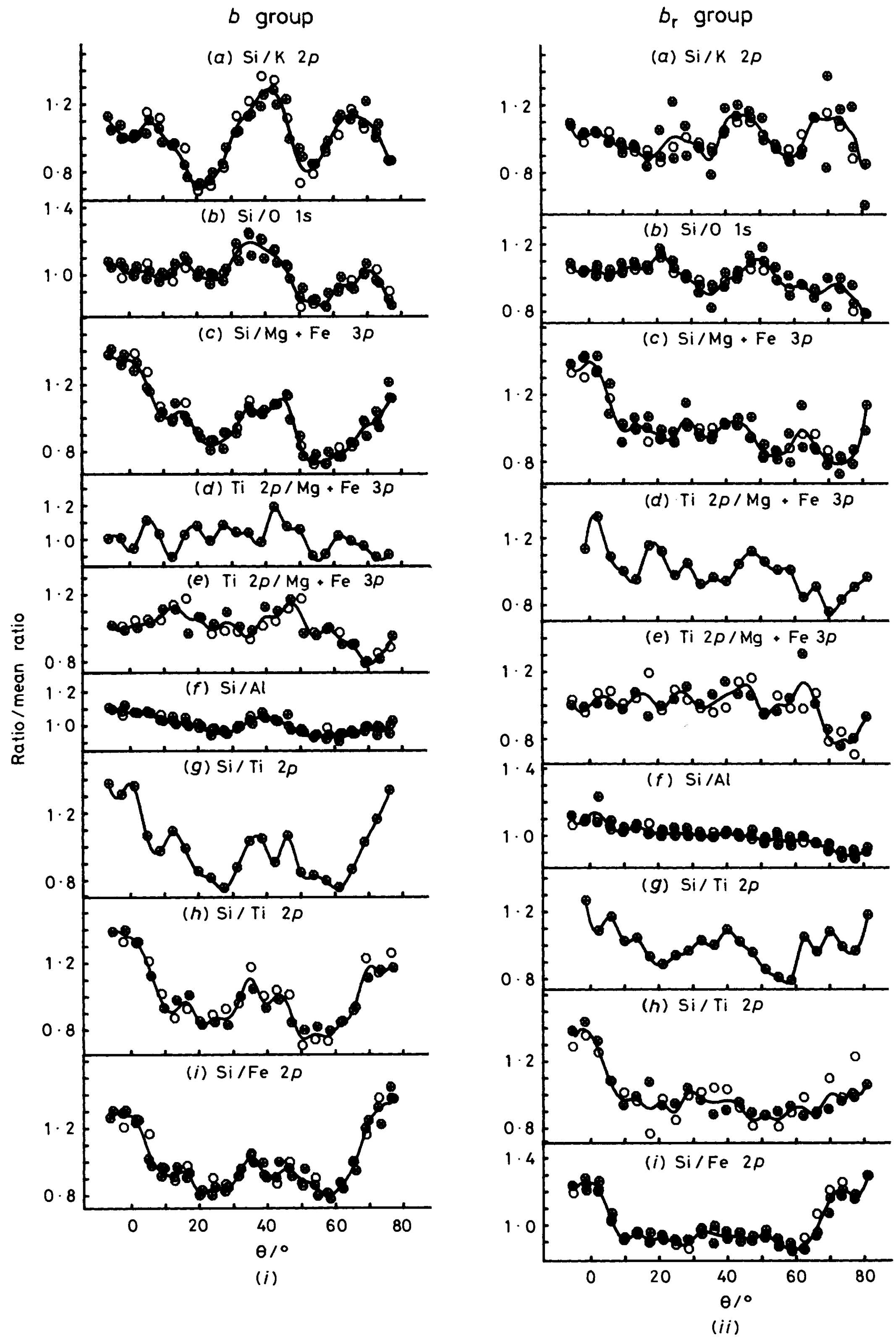

Figure 6. Biotite x.p.d. patterns for the *b*-group rotations. In (*i*) the three symbol types (1—3) relate to the *b*′, *b*, and *b*″ rotations respectively, in (*ii*) to the b_r', b_r, and b_r'' rotations respectively

given incident photon flux, the total number of primary photoelectrons produced should be independent of θ, since diffraction of the incident photons ($\lambda \approx 10$ Å) can be neglected.[9] Because most of the photoelectrons are inelastically scattered a number of times before emerging from the solid, and are likely to be deflected to some extent on each collision, the anisotropy of the background photoelectron angular distribution should become progressively less marked as the energy

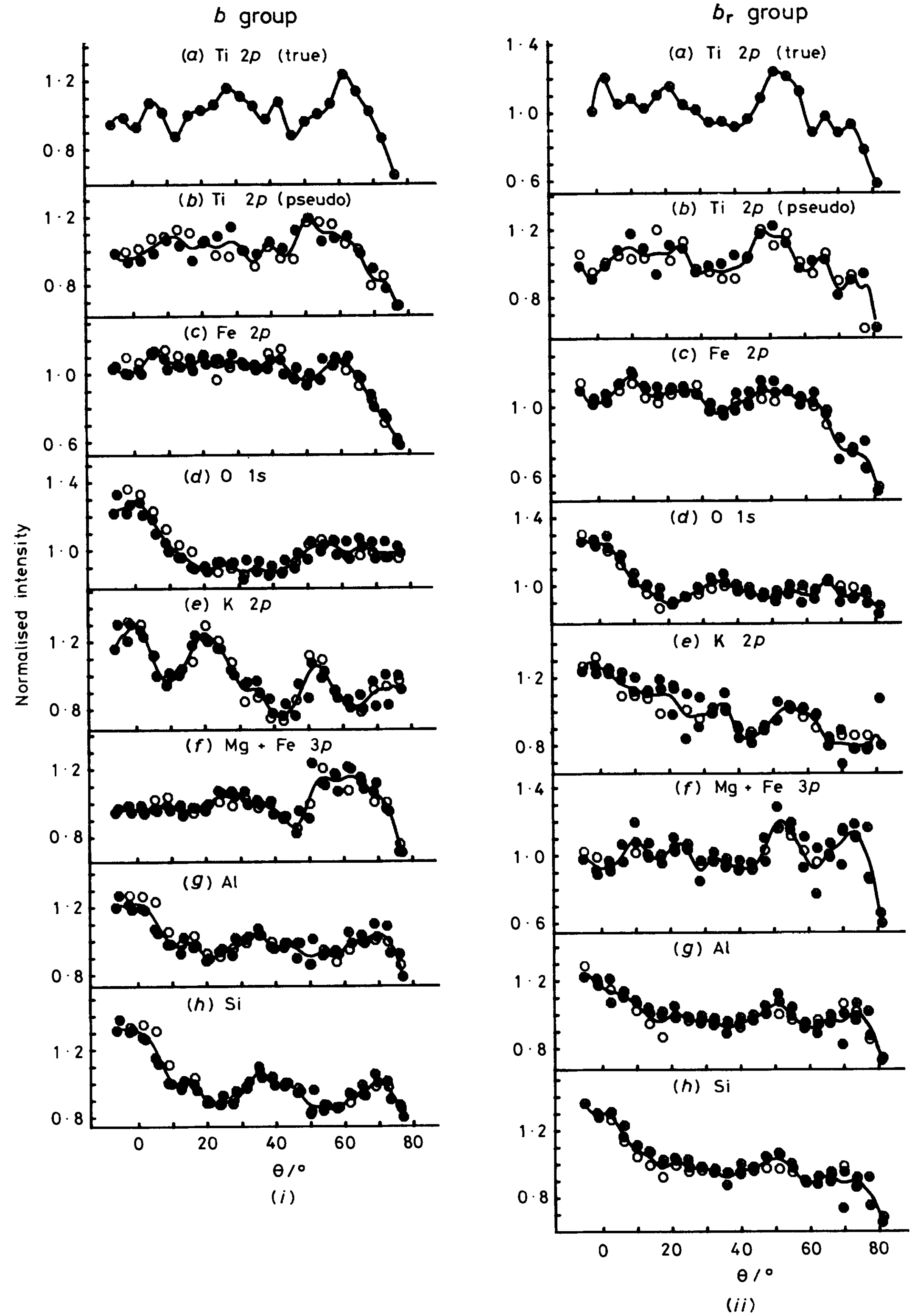

Figure 7. X.p.d. curves corresponding to the patterns in Figure 6, for the *b*-group rotations in the biotite

sampled is decreased, *i.e.* the number of inelastic scattering events suffered by the electrons is increased. It is thus reasonable to expect that the background at energies well below the primary energy should not be significantly modulated by x.p.d. effects. Now, in each set of spectra (Figure 2), most of the recorded background does not originate from the peak superimposed on it, but from peaks at much higher k.e.s: this background in total thus should be negligibly modulated by x.p.d. The background is however still proportional to the integrated photon flux, and to the detection efficiency (a complicated function of experimental geometry[9]).

Consequently, by integrating the background after subtrac-

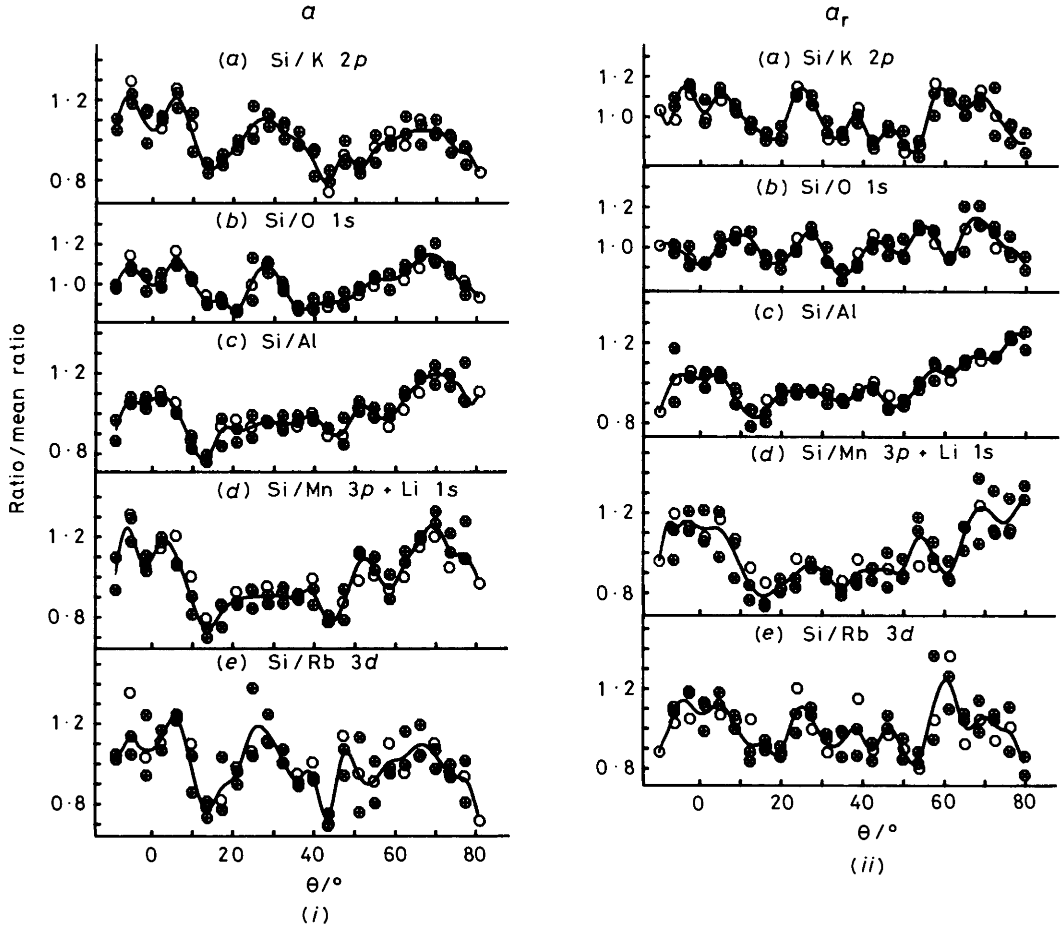

Figure 8. Lepidolite x.p.d. patterns for (*i*) the *a* and (*ii*) the a_r rotations. Symbol types 1 and 2 relate to data from the crystal used to obtain the *b*-group results shown in Figures 12—15; symbol type 3 denotes data from a second crystal, that used when collecting the data shown in Figures 10 and 11. The two crystals were cleaved from a common parent, and the duplicate data sets were not collected immediately following the initial set

tion of the elastic peak intensities a normalising factor for a group of spectra as a whole can be obtained. This factor is plotted as a function of θ for two typical data sets in Figure 2(*e*) and (*f*); the x.p.d. modulation is, as expected, essentially absent. Individual peak intensities were therefore calculated by dividing the net peak intensity by the normalising factor, and then dividing by the mean corrected intensity (over all angles). Plots of corrected intensity *vs.* θ then reveal the extent of x.p.d. modulation independently of the mean intensity of the peak concerned relative to the others.

One small error in the correction process arises from the contribution to the spectra from the carbon coating of the sample mounting. The extent of this contribution varied to some extent with the precise positioning of the probe in relation to the analyser entrance slit, a high Aquadag contribution leading to a spuriously high normalising factor. Variations in the extent of carbonaceous contamination of the sample surface itself will also affect normalising factors obtained by this procedure: high levels of contamination lead to both an increased normalising factor and a reduced count rate from the mica, and hence to a low value for the corrected peak intensity. No systematic effects arising from either source were identified, but such effects nevertheless probably contributed to the significantly poorer reproducibility of plots of normalised intensity against θ (in comparison with plots of ratios between intensities) evidenced in the data reported below.

Results and Discussion

We shall throughout be making deductions from quite subtle differences between x.p.d. patterns. We have found it most helpful to use transparent overlays of one diagram on another, and to aid this, all the data are reproduced on the same scale. Because the observation of resemblances between x.p.d. patterns tends to be subjective, we also quote, where appropriate, correlation coefficients between the relevant patterns. Thirty points taken at equal intervals over the central 60° of the mean curves shown in the diagrams were used in each such comparison. However, such coefficients must be interpreted carefully, as, in effect, the points in any pattern most deviant from unity are the most heavily weighted. They are thus unreliable as a quantitative measure of resemblance wherever the anisotropy represented by the x.p.d. pattern is small relative to the (random) uncertainties in the data. Correlation coefficients are thus a supplement to, rather than a substitute for, a study of the patterns themselves.

Results and Initial Symmetry Considerations.—Figure 3 shows the results from the biotite for the two rotation axes parallel to *a*: the data for *a* and a_r were found not to be significantly different and so were plotted together. The data for the four pseudo-*a* axes (shown in Figures 4 and 5) were very similar, but the patterns for a' and a_r'' were not quite identical with those for a'' and a_r' [compare (*i*) and (*ii*) in Figures 4 and 5 respectively].

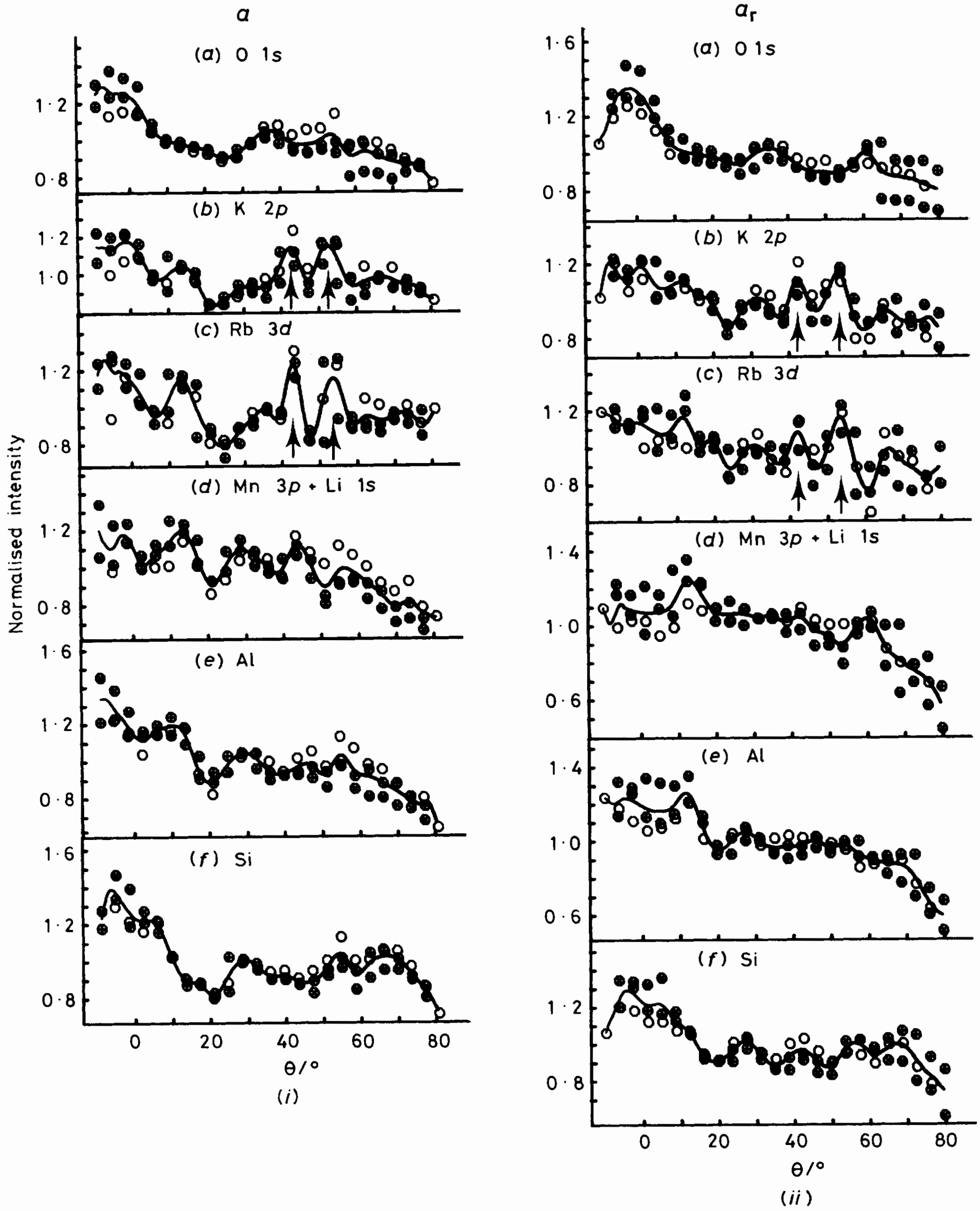

Figure 9. X.p.d. curves corresponding to the patterns in Figure 8

Plots of normalised individual peak intensities against θ, which we refer to as 'x.p.d. curves' to distinguish them from the plots of peak intensity ratios previously described as 'x.p.d. patterns,' are shown in Figures 3(*ii*) and 5.

Identity of the *a* and a_r data is expected in *C*2/*m* symmetry and inspection of Figure 1(*a*) or a model shows that the observed 'pairing' of the pseudo-*a* data is also a reflection of the crystal symmetry. The slight but distinctive differences between (*i*) and (*ii*) in Figures 4 and 5 arise because planes perpendicular to the cleavage and parallel to a pseudo-*a* axis are not crystallographic mirror planes. The marked differences in the titanium data will be discussed later. The general similarity of the major-element *a* and pseudo-*a* data confirms that short-range effects are usually dominant, because the immediate environments of corresponding emitters are identical. However, there are significant differences between the *a* and pseudo-*a* data for the interlayer ion (K^+): the *a* and a_r K 2*p* x.p.d. curves show pronounced peaks near 41 and 52° (arrowed, Figure 3) which are absent from all the pseudo-*a* curves. These peaks also feature in the lepidolite data: they must arise from effects due to more distant neighbours, present in relation to the *a* axis but not the *a*′ or *a*″ axes. However, if these features are associated with individual scatterers the *nearest* possible atoms (Si) are as much as 10.7 and 13 Å from the emitting sites. Clearly, long-range effects cannot always be neglected.

The *b*-group data for the biotite are reproduced in Figures 6 and 7. As expected, azimuthal rotation through 180° now causes gross changes in all the patterns (such pairs of rotations in the *b*-

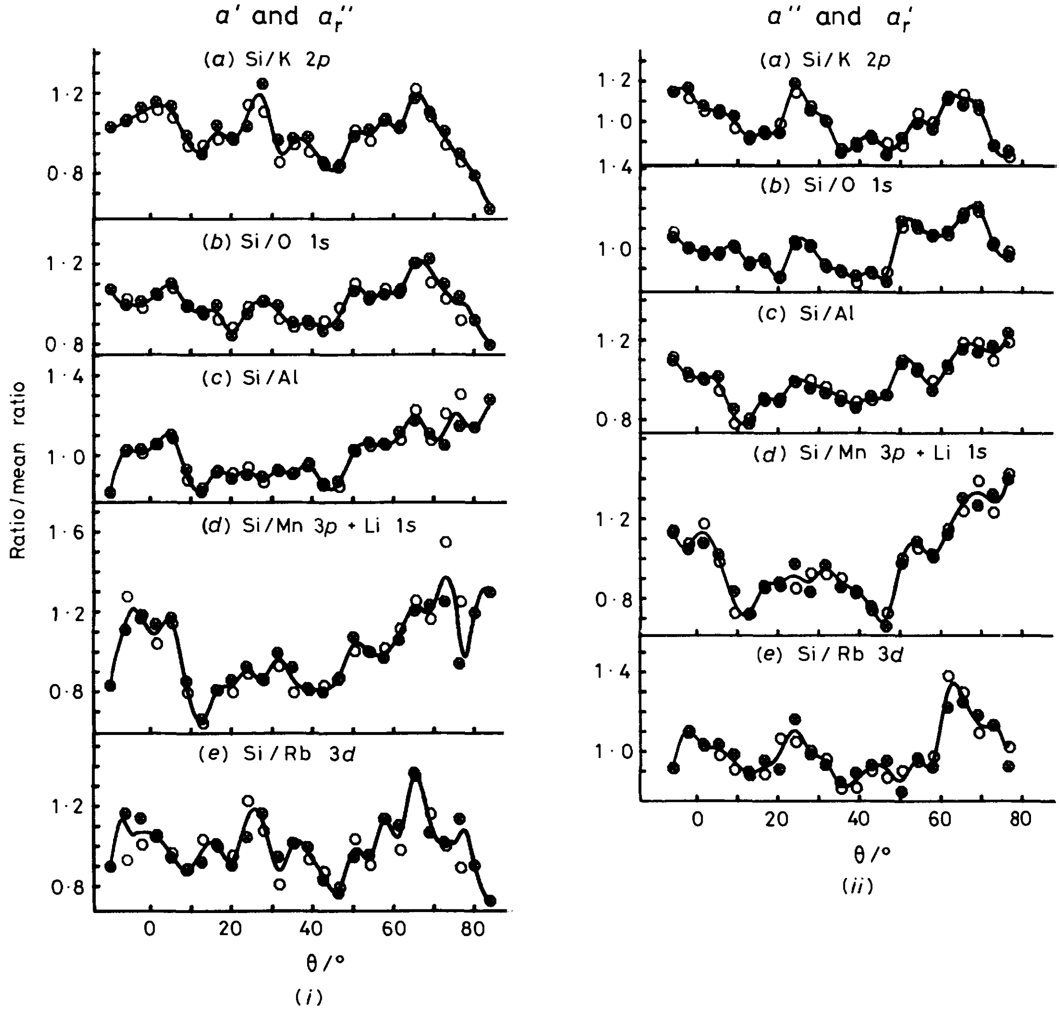

Figure 10. Lepidolite x.p.d. patterns for the pseudo-*a* rotations. In (*i*) symbol types 1 and 3 relate to the a' and a_r'' axes respectively, in (*ii*) to rotation about a'' and a_r' respectively

group are not symmetry-equivalent) but in the major-element patterns the true- and pseudo-*b* rotation axes cannot be distinguished within each set. The recorded differences between the pairs of pseudo-*b* and -b_r data, which are in each case symmetry-equivalent, are as great as those between these pairs and the true-*b* and -b_r data respectively. For example, the mean correlation coefficient between b' and b'' for (*a*), (*b*), (*c*), and (*i*) in Figure 6(*i*) is 0.87 whereas that for the same comparisons between *b* and b', b'' is 0.92. The *b*-group patterns must thus be essentially determined by short-range effects, to an even greater extent than the *a*-group patterns. For Ti, however (see below), we shall show that certain of the differences between the true- and pseudo-*b* axes are significant; for this element only, the plots have been separated.

The Fe 2*p*, Ti 2*p*, and K 2*p* *b*-group patterns show no systematic drift with angle (suggestive of a near-surface concentration gradient[4,8]); the trends in Figure 3 which might have been held to suggest surface depletion of Fe, and, to a lesser extent, Ti and K, must therefore actually be due to x.p.d. effects.

The lepidolite data contrast quite strongly with those for the biotite, although the basic structures of biotite and lepidolite are virtually identical.[17] The *a*-group data are shown in Figures 8—11. Again there are close parallels both between the data for the different near-equivalent rotation axes, and between these data and those for the corresponding rotations for the biotite (Figures 3—5). However, there are now marked differences between *a* and a_r: compare Figure 8(*i*) with (*ii*), (*a*) and (*b*) especially. The lepidolite thus cannot have *C*2/*m* symmetry: the mirror plane is absent. The peaks mentioned above for K in biotite near 41 and 52° are nevertheless again present in both *a* and a_r for K and Rb (arrowed, Figure 9), but not in any of the pseudo-*a* data. As for the biotite, differences within the pseudo-*a* group are not large. The two non-equivalent rotations represented by a' or a_r'' and a'' or a_r' are nevertheless again differentiated. The distinction is subtle, but successive superposition of sections of Figures 4 and 10 reveals the parallels clearly, especially the consistent differences in the profiles of the Si/K patterns between 0 and 50° and in those for Si/O between 50 and 60°. The mean correlation coefficient between the x.p.d. patterns from biotite and lepidolite for 'matching' orientations are 0.80 for Si/K 2*p* and 0.92 for Si/O 1*s*, *cf.* 0.61 and 0.81 respectively for comparisons in the opposite sense.

The *b*-group data for the lepidolite are illustrated in Figures 12—15. The *b* and b_r data here are throughout clearly differentiated from the corresponding pseudo-*b* data. Since the biotite data were so similar for each trio of *b*-group axes, this differentiation indicates that in the lepidolite, unlike the biotite, there are differences in environment very close to the emitting sites. Specifically, the only plausible cause is ordering of the Li, Mn, and Al cations in the octahedral sites, thus removing the

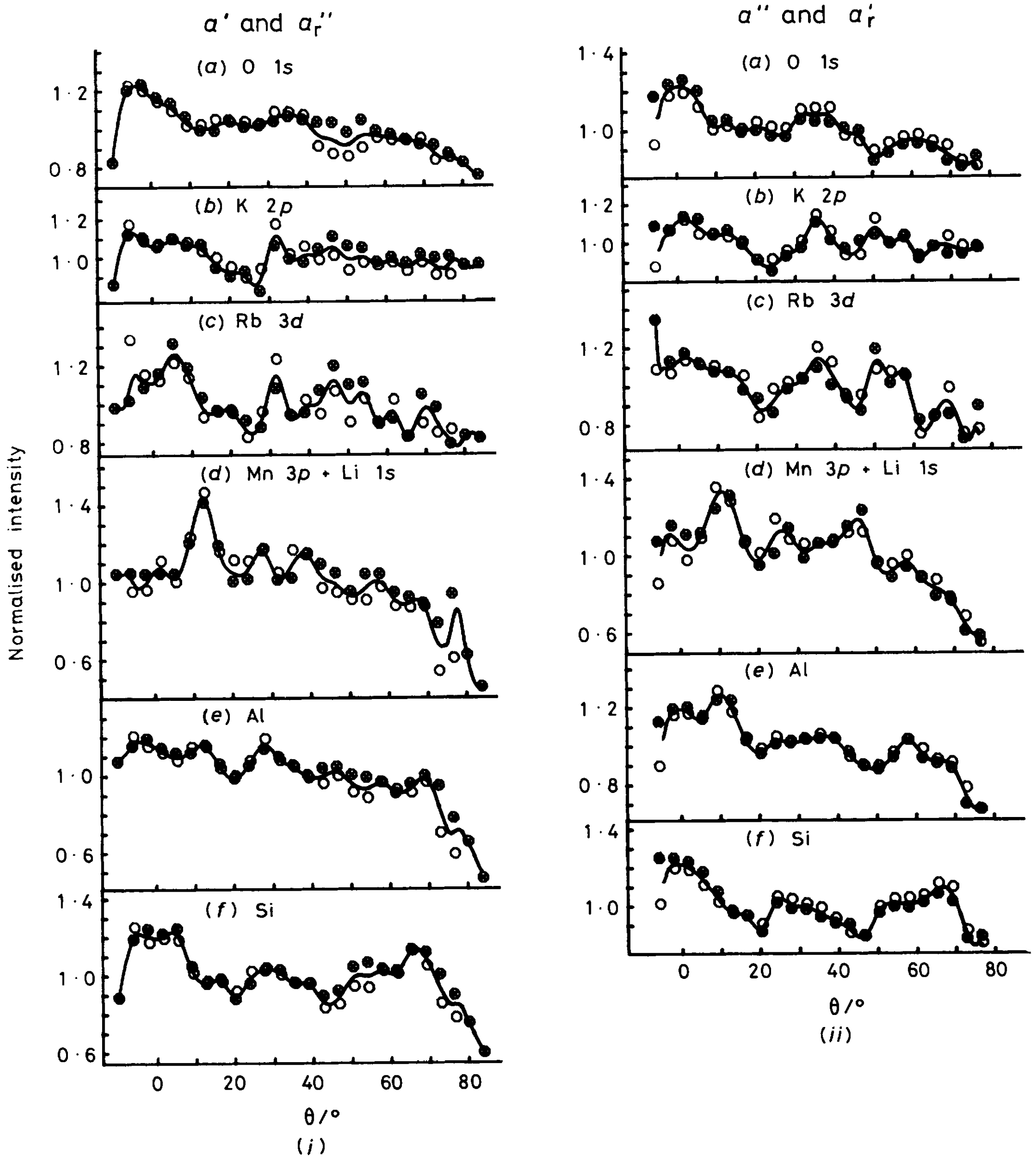

Figure 11. X.p.d. curves corresponding to the patterns in Figure 10

three-fold symmetry of the octahedral sheet. This is discussed in detail below.

This difference between the micas is not due simply to poorer crystal quality in the biotite. The consistent presence of the two sharp features in the K, Rb patterns at θ = 41 and 52° (discussed above) which distinguish all eight sets of true-*a* from the eight sets of pseudo-*a* data confirms the basic structural integrity of both crystals.

The aluminium curves in biotite resemble the corresponding silicon curves, because 70% of the Al occupies tetrahedral (Si) sites.[6,10] In the lepidolite, only 34% of the Al is tetrahedral and the similarities between the curves for Al and Si are much less marked. The aluminium curves here are not, however, merely weighted sums of those for Si and Mn,Li: the aluminium sites are clearly distinct, in part, and we shall return to this point later.

Even a tentative identification of particular peaks in the x.p.d. curves with particular scatterers is rendered difficult by the inherent complexity of the mica structure. Using Guggenheim's[27] *X*-ray data for a lepidolite of similar composition, we have generated histograms representing the near neighbours of each element as a function of θ. Atoms more than 7.5 Å away were neglected and the contributions of the nearer atoms weighted inversely with internuclear separation. Neighbours centred > 1 Å off the normal to the rotation axis passing through the emitting atom were also neglected. Typical histograms, for the *b* and b_r rotations, are compared with the x.p.d. curves in Figure 16. Some features show a correlation; the angular gaps in the histograms match the principal minima in the x.p.d. curves quite consistently, but the x.p.d. maxima are not well predicted. Overall, the correlation is not remarkable and it is clear that this simplistic approach is inadequate. Preliminary calculations[16] confirm that atoms within a 60° cone from the electron emission site affect the intensity significantly.

Comparison with Previous X.P.D. Studies.—The present Laue photographs show that the lepidolite x.p.d. data reported previously[6] were obtained by rotation about the true *b* axis,

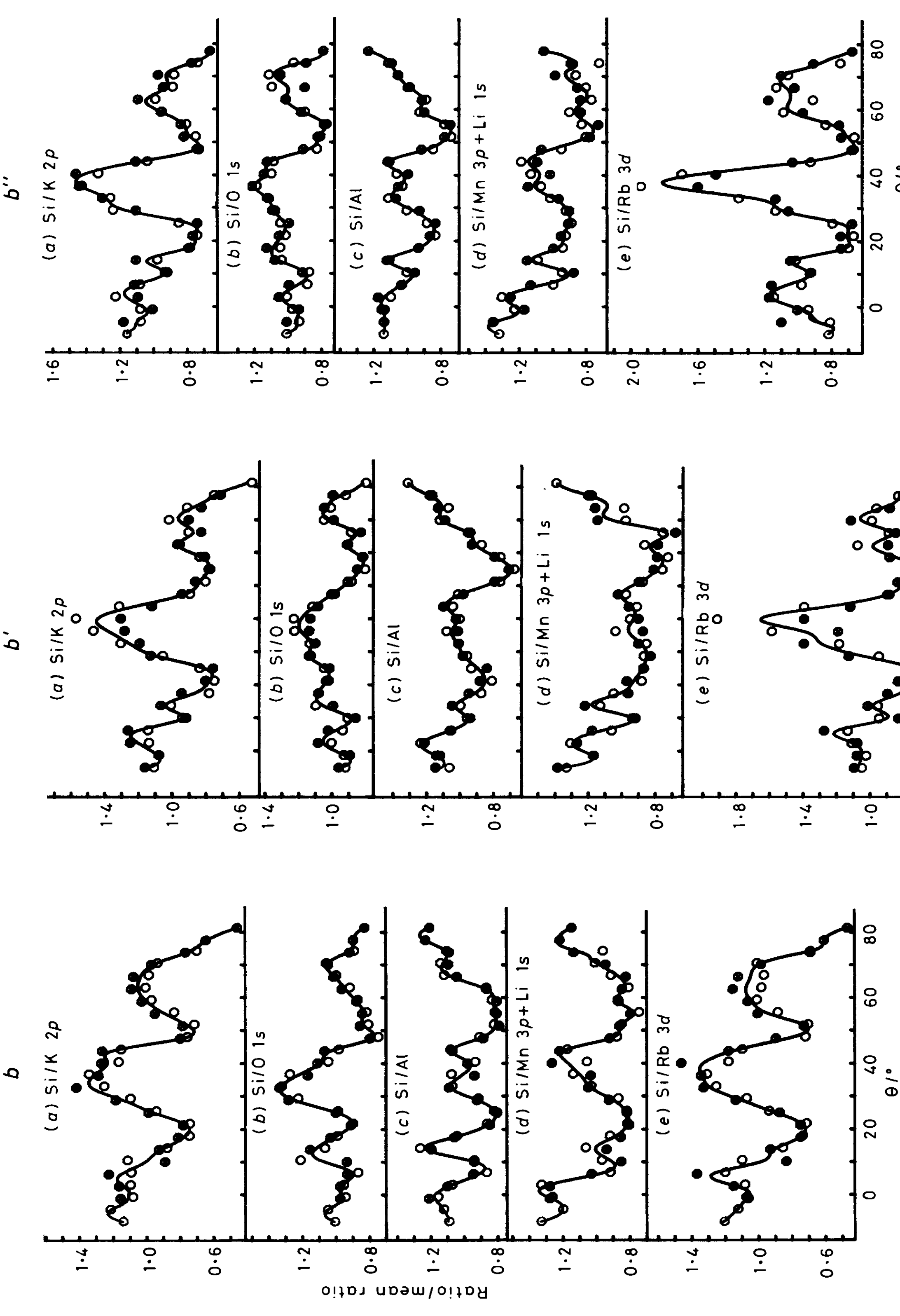

Figure 12. Lepidolite x.p.d. patterns for the *b*-group rotations: (*i*), (*ii*), and (*iii*) denote data from rotation about the *b*, *b*′, and *b*″ axes respectively. In each case symbol types 1 and 3 distinguish two sets of data from the same cleavage surface; duplicate data sets were not collected immediately following the initial sets

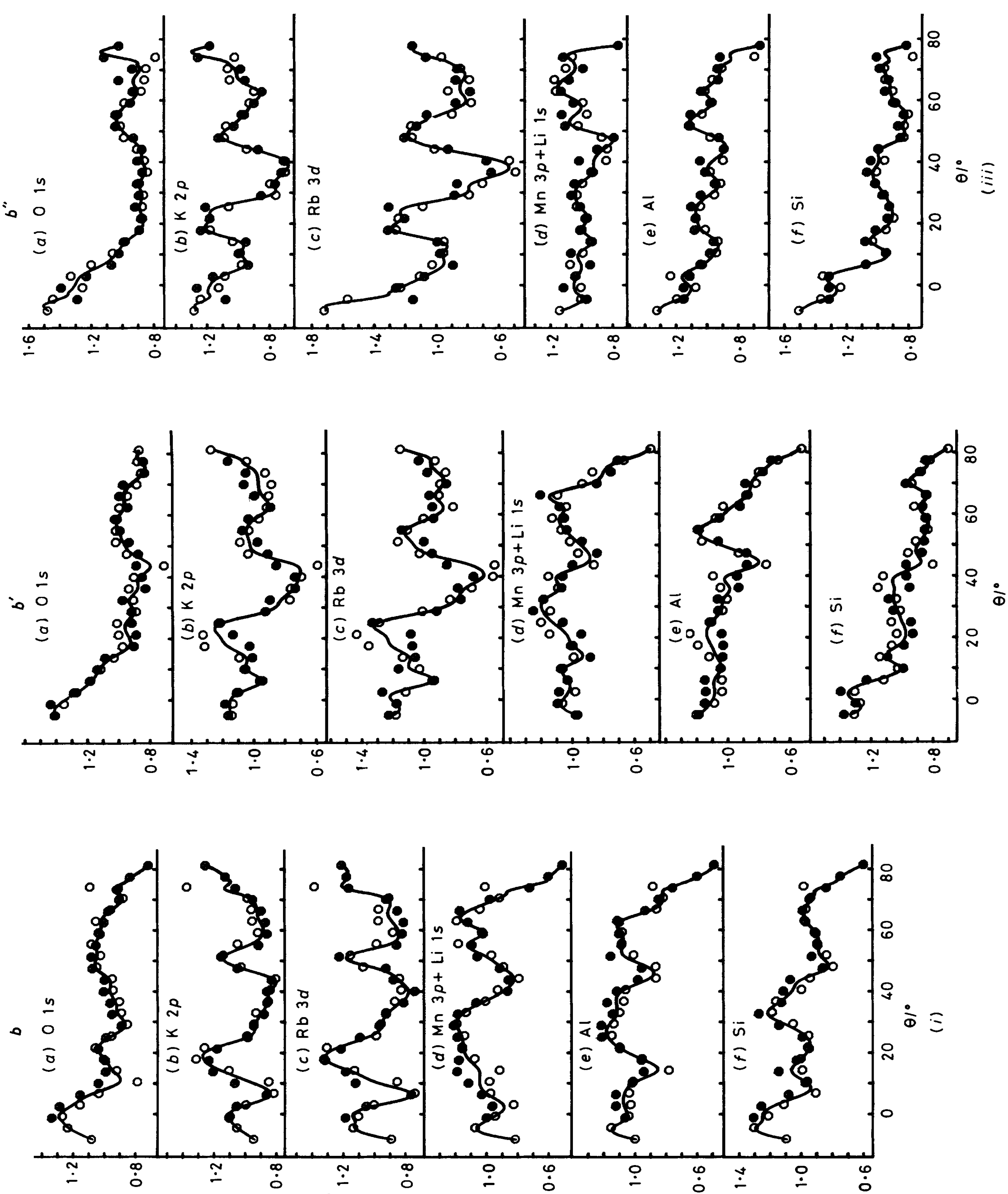

Figure 13. X.p.d. curves corresponding to the patterns in Figure 12

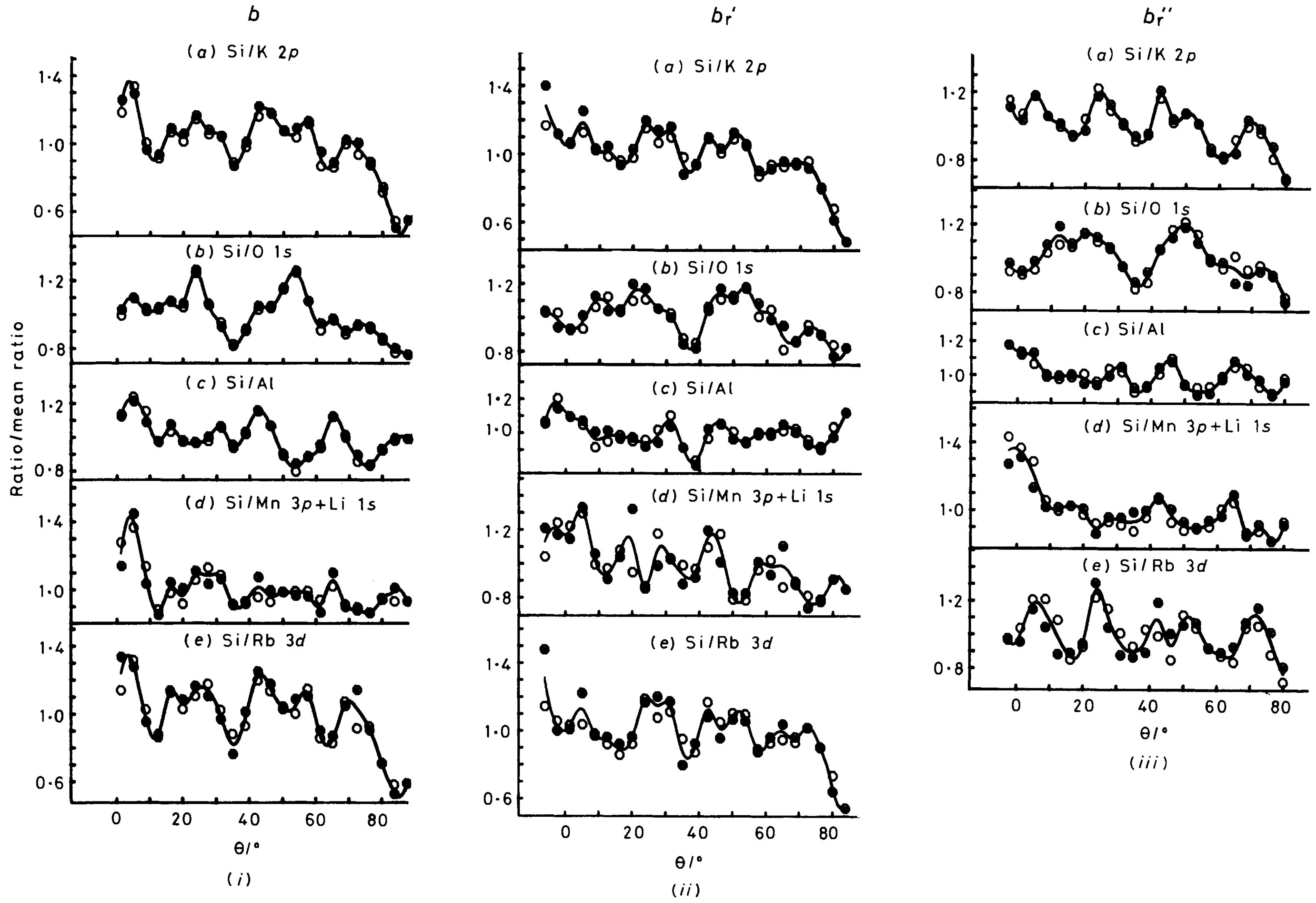

Figure 14. Lepidolite x.p.d. patterns for the *b*-group rotations. In (*i*) symbol types 1 and 3 relate to two data sets obtained by rotation about the b_r axis, from the same surface. The duplicate data set was not collected immediately following the initial set. In (*ii*) symbol types 1 and 3 relate similarly to b_r' rotation and in (*iii*) to b_r'' rotation

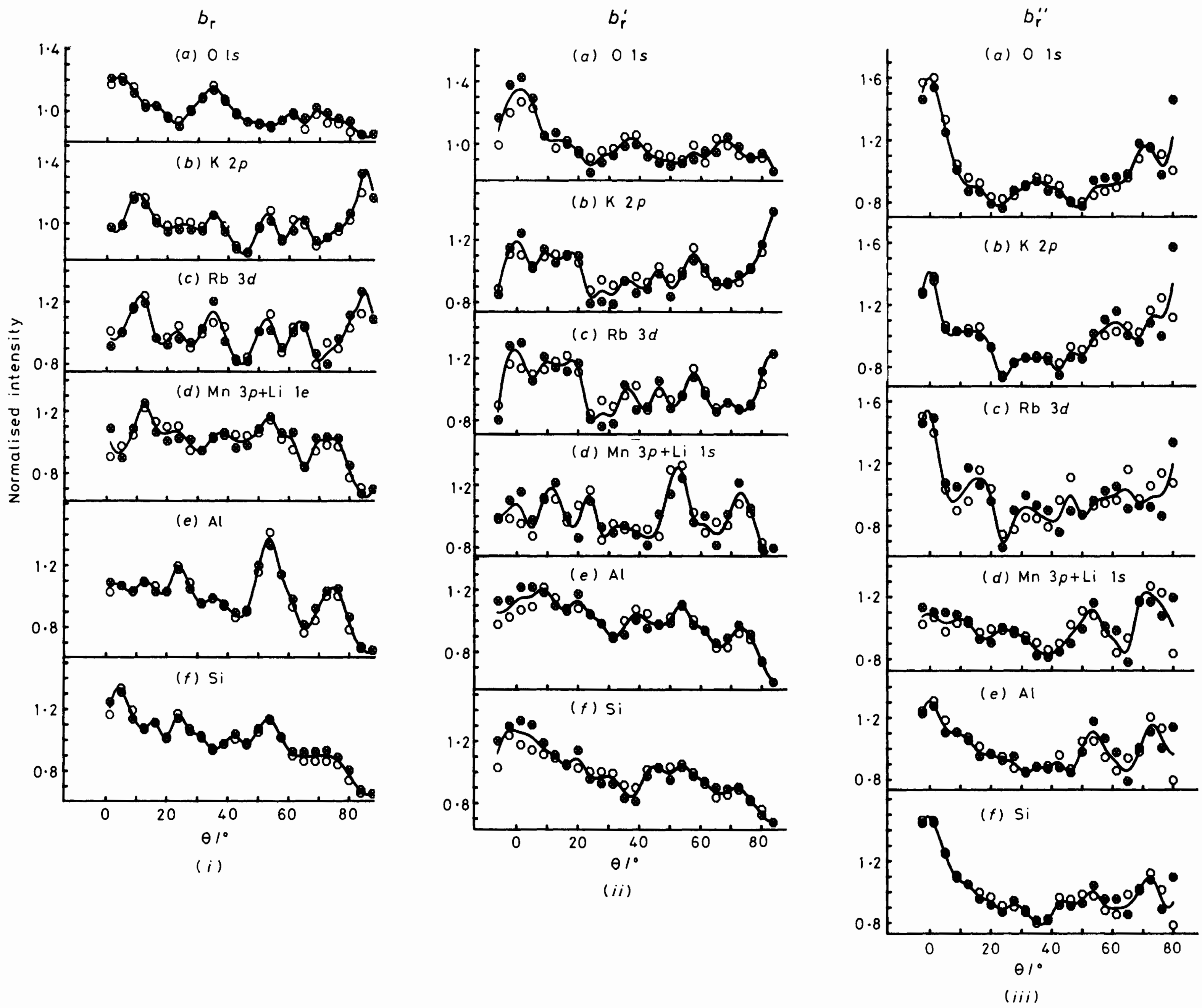

Figure 15. X.p.d. curves corresponding to the patterns in Figure 14

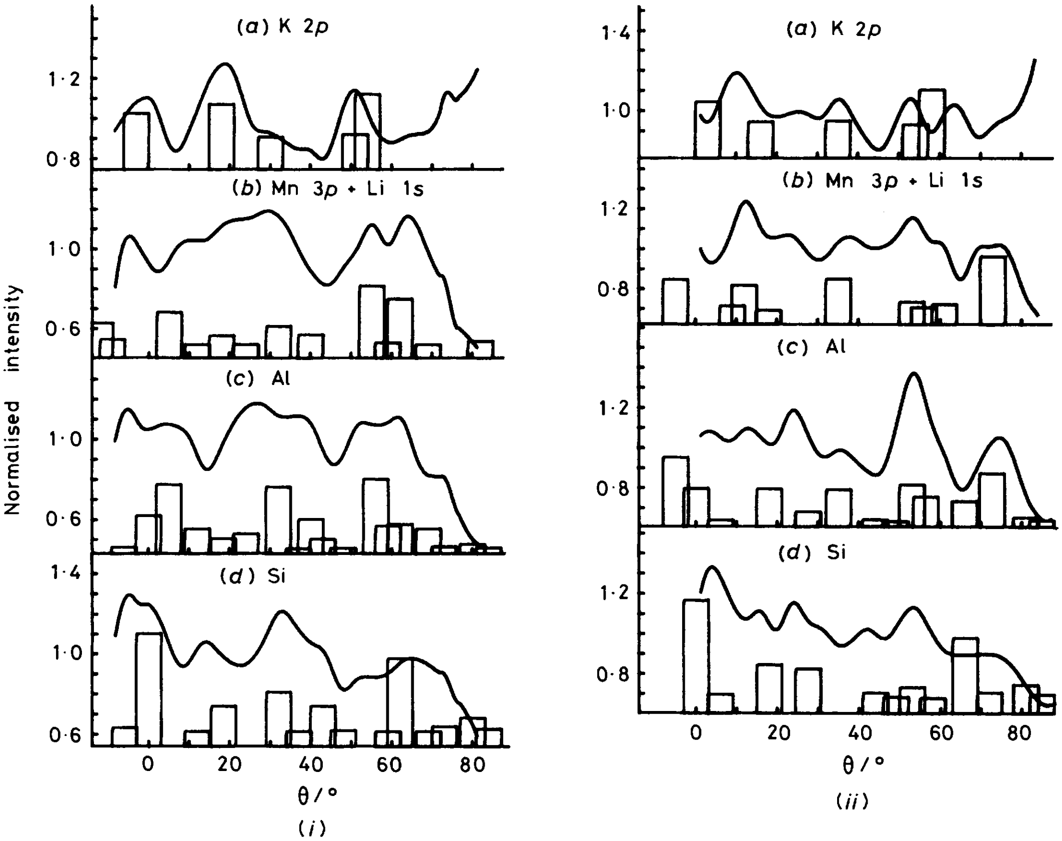

Figure 16. Comparison of (*i*) *b* and (*ii*) b_r x.p.d. curves for the lepidolite [mean lines from Figures 13(*i*) and 15(*i*)] with near-neighbour histograms derived from Guggenheim's[27] *X*-ray data. Wherever two scatterers were within 2° of the same direction the bar heights have been added as an aid to clarity

while in the experiments on biotite[7,8] rotation was about a pseudo-*b* axis. The oscillation photographs taken in the previous studies to determine crystal orientation did not enable the *b* and pseudo-*b* axes to be distinguished. For both micas, the present data, where they duplicate previously reported data [Figures 6(*i*) and 12(*i*) only], confirm the original results. The improved data-processing techniques have enabled the interference between Rb 3*d* and the Al 2*s* $\alpha_{3,4}$ satellites[6] (see Figure 2) to be eliminated so that the present Rb 3*d* data match the previous Rb 3*p* patterns quite closely.

Interlayer Ions: Rb^+ *sites in Lepidolite.*—It was noted previously[6] that the absence of any progressive increase in the Rb/K ratios at high take-off angles demonstrates that the Rb^+ ions are not segregated into rubidium interlayers, but are uniformly distributed amongst the K^+ ions. The present data for all rotation axes confirm this, but the additional data also reveal that the Rb 3*d* patterns are consistently more anisotropic than those for K 2*p* (see especially Figures 9 and 12). The Rb 3*d* photoelectrons, at *ca.* 1 137 eV k.e., have a slightly shorter de Broglie wavelength (0.37 Å) than the K 2*p* photoelectrons (0.40 Å), and hence a smaller Bragg angle. Using the Kikuchi-band approach, Rb 3*d* x.p.d. peaks should then be somewhat sharper than those for K 2*p*. We attribute the enhanced anisotropy partly to this effect. However, Rb 3*p*, very close in k.e. to K 2*p*, also yielded[6] a pattern showing small differences from the K 2*p* pattern. Some of the difference between the Rb 3*d* and K 2*p* must therefore be due to other factors, such as the increased mass (*ca.* × 2) of Rb^+ relative to K^+, which presumably reduces the amplitude of thermal vibration for the heavier ion. The greater size of Rb^+ may also be important.

Cation Ordering in the Micas.—There is an increasing interest in the characterisation of both octahedral and tetrahedral cation ordering in the micas.[17,18,28,29] Ordering is of considerable geochemical importance, but it is only relatively recently that crystallographic and other techniques capable of providing reliable results have become available. *X*-Ray methods, which only detect long-range order, have been used extensively to characterise the distribution of ions between the three octahedral cation sites, M(1) with *trans*-OH groups lying in a mirror plane of the ideal *C*2/*m* structure, and M(2) and M(3), both with *cis*-OH groups. In the ideal structure the latter are crystallographically equivalent, located symmetrically on either side of the mirror plane. Proven examples of octahedral ordering in biotite are rare, but in lepidolite segregation of the larger cations, principally Li, into the M(1) *trans* sites is quite common.[28,29] Sometimes, but not always, this is accompanied by a further segregation of one of the remaining ions, generally Al^{3+}, into one of the two *cis* sites.[27–29] In the latter case, the mirror plane is lost, and the space group reduces to *C*2.

Studies of tetrahedral ordering by *X*-ray methods, unlike those by neutron-diffraction techniques,[30] are hindered by the closely similar scattering powers of Al and Si, and much recent work[31–36] has used magic-angle spinning nuclear magnetic resonance (m.a.s.n.m.r.). The information obtained differs from that given by *X*-ray methods in that it relates only to short-range order, so that domain models may be considered; but as it is also limited to distinguishing the numbers of Al and Si nearest neighbours, unambiguous determination of the complete structure of the tetrahedral sheet is not usually possible.

X.p.d. can in principle be applied in the study of both tetrahedral and octahedral cation ordering. While not giving long-range information in the sense that *X*-ray diffraction does,

Table 2. Distribution of octahedral cations between '*cis*-like' (C) and '*trans*-like' (T) sites in lepidolite in comparison with correlation coefficients between x.p.d. patterns. R, R_r = Correlation coefficients for indicated pairs of b-group and b_r-group patterns respectively

Pattern*	b',b''_r rotation	% Sites common, R, R_r	b, b_r rotation	% Sites common, R, R_r	b'', b''_r rotation
Si/Mn,Li	1.00C	44%, 0.60, 0.66	0.56T + 0.44C	44 + 44 = 88%, 0.89, 0.72	0.44T + 0.56C
		100%, 0.63, 0.89		61%, 0.85, 0.67	
		73%, 0.87, 0.56		56%, 0.72, 0.82	
Si/Al	0.83T + 0.17C	17%, 0.69, 0.45	1.00C	83%, 0.86, 0.82	0.17T + 0.83C
%Sites common, R,R_r	17%, 0.72, 0.56		44%, 0.66, 0.64		17 + 56 = 73%, 0.88, 0.75

* The patterns for the octahedral ions relative to Si are used rather than the x.p.d. curves themselves to eliminate the contribution from tetrahedral Al.

it is nevertheless necessary that the emitting sites be similarly oriented over a very large distance (up to several mm). Domain structures over which the long-range average is effectively the ideal (disordered) structure will not be detected.

X.p.d. has been shown to be sensitive to nearest-neighbour directions in relation to the rotation axis,[13,37] and thus the two sets of cations at the centres of alternate tetrahedra round each six-cation ring should in principle give rise to different a-axis x.p.d. patterns. Ordering of Al into one of these sets is relatively difficult to study by *X*-ray crystallography, because of the necessarily increased size of the unit cell (all the tetrahedra are symmetry-equivalent in $C2/m$). The m.a.s.n.m.r. results suggest that such ordering does sometimes occur in the 2:1 layer silicates.[31–36] If present in the micas studied here, it would be most obvious in comparison of the a and a_r aluminium patterns: the 180° azimuthal rotation would effectively interchange the Al between the two orientations distinguished by x.p.d. (*cf.* Zn and Se in ZnSe, where, for the appropriate axis, the patterns for Zn and Se interchange on 90° rotation[37]). A pronounced difference between the two aluminium curves would thus be expected. No such effect is evident in any of the data reported here. Moreover, tetrahedral ordering could only significantly affect Al and Si photoelectron angular distributions. The scattering powers of Al and Si are so similar that effects on the angular distribution of photoelectrons originating from any other element in the structure would be negligible. The lack of equivalence between the a and a_r data for lepidolite, much more obvious in the Si/K and Si/O ratios than in Si/Al, cannot therefore be due to tetrahedral ordering.

This absence of the expected mirror plane must therefore demonstrate, instead, an inequivalence of the *cis* M(2) and M(3) sites, *i.e.* that the octahedral cations order in three sites in this lepidolite, as in, *e.g.*, the Tanakamiyama specimen studied by Guggenheim.[27] Analogous segregation in our lepidolite would imply an octahedral composition of M(1) $Li_{0.83}Mn_{0.17}$, M(2) $Li_{0.66}Mn_{0.13}Al_{0.21}$, and M(3) $Al_{1.0}$ with a consequent difference in scattering power between M(2) and M(3). The two *cis* sites are not x.p.d.-equivalent for the a-axis rotations, the 180° azimuthal rotation between a and a_r interchanging M(2) and M(3). Consequently, somewhat larger differences should occur between the x.p.d. data for Mn,Li than for Al (see Figures 8 and 9). *A priori*, Al could be concentrated in either *cis* site: the above assignment, with M(3) defined as in Figure 1(*a*), was deduced from the interpretation of the b-group data given below.

As for the biotite, long-range effects necessitate the pairing of the pseudo-a data (a' with a''_r and a'' with a'_r) to accord with the basic symmetry of the structure. (In other pairings the internal consistency is much less satisfactory and no distinctions between any of the pseudo-a rotations are then possible.) The patterns for Al and Mn,Li in each plot are different from each other, and features of the a',a''_r Si/Al pattern (notably the pronounced dip near 47°) transfer to the a'',a'_r Si/Mn,Li pattern, while the broader minimum centred at 42° interchanges between a',a''_r Si/Al and a'',a'_r Si/Mn,Li. Azimuthal rotations through 120° in effect sequentially exchange the three sites, the *trans* M(1) site in a transforming into a near-equivalent of a *cis* site in the pseudo-a rotations and one of the *cis* sites similarly becoming '*trans*-like;' the differences are relatively small since the immediate oxygen co-ordination shell is similarly oriented in each case. Cation ordering thus provides a simple explanation of the observed interchange of features. If the octahedral cations were randomly distributed amongst the three sites the patterns for Al and Mn,Li would have been virtually indistinguishable throughout. However, to produce such effects it is necessary only for the occupancy of the *trans* site to be distinctly different from that of the *cis* sites, and not for the latter also to be differentiated from each other. The only confirmatory evidence from these plots for the differentiation of M(2) from M(3) would be an imperfect matching of the pairs of pseudo-a data sets plotted together; in the absence of such differentiation they would be rigorously symmetry-equivalent. In fact, no significant differences were observed.

However, confirmatory evidence for the segregation of Al into one of the two *cis* sites can be derived from the b-group patterns. The close similarity of the b' data with those for b'' (and b'_r with b''_r), contrasting with b and b_r respectively, indicates that the major effect of cation ordering on these x.p.d. patterns also is due to the differentiation of the two *cis* sites from the *trans*; several *X*-ray studies[17,18,27–29] have shown that the *trans* M(1) site is enlarged to accommodate the larger cations, with loss of the three-fold symmetry of the octahedral sheet. The resultant difference in mean scattering power between the ions occupying the *cis* and *trans* sites is probably also significant. Ordering of the cations additionally between the two *cis* sites [M(2) and M(3)] causes more subtle effects, which manifest themselves principally in the residual differences between b' and b'' (and b'_r and b''_r). These effects can be detected only in the patterns for the octahedral ions themselves; even there they are not dramatic, because the six nearest-neighbour oxygen atoms are similarly oriented around all three sites. Nevertheless, there is evidence here not only to confirm that the Al segregates into one of the two *cis* sites, but also to show that it is the M(3) site which is aluminium-rich.

The contribution of '*cis*-like' (C) and '*trans*-like' (T) sites to the patterns for Mn,Li and Al in the b', b'_r and b'', b''_r orientations in comparison with b,b_r can be deduced immediately (Table 2) from Figure 1(*a*) and the octahedral ion distribution given above. Also shown in Table 2 are the correlation coefficients between each pair of patterns, to compare with the percentage of approximately common sites. Note that, because of the distortion induced by the increased size of the M(1) ions, it is not unreasonable that the correlation coefficient between, *e.g.*, Al in b and Mn,Li in b' should be only 0.63 for an assumed 100% of common sites: correlation coefficients between b,b_r and b',b'_r or b'',b''_r patterns respectively for the non-segregated elements K and O range from 0.46 to 0.82 with a mean of 0.70.

Three significant groups of correlations may be identified. First, the patterns for Si/Mn,Li and Si/Al should be much more closely correlated for b'' and b''_r than for b' and b'_r or b and b_r, as indeed is the case. Secondly, both Si/Al and Si/Mn,Li patterns for b,b_r should correlate more closely with those for b'',b''_r respectively than with those for b',b'_r; this is found for all four comparisons of this type. Finally, b,b_r Si/Al should correlate better with b',b'_r Si/Mn,Li than with b',b'_r Si/Al, *etc.*; this expectation is fulfilled in six of the eight such 'diagonal' comparisons between b,b_r and b',b'_r in the Table. Many of these observations can also be made qualitatively (but more subjectively) by inspection of Figures 12—15.

If Al were concentrated in M(2) rather than M(3) the contributions under b',b'_r and b'',b''_r in Table 2 would be interchanged. This alternative assumption of aluminium concentration in M(2) leads to a strong negative correlation between R and the percentage of common sites. Overall, the evidence seems conclusive: Al in this lepidolite is strongly concentrated in the M(3) site. The octahedral ion distribution given above was therefore adopted when calculating the histograms for Figure 16. However, the quantitative extent of segregation cannot yet be confirmed by x.p.d.

The lack of distinction within each set of three *b*-group patterns for biotite is readily explained on a similar basis. If Fe^{2+} and Mg^{2+} do not order, possibly because they are similar in size and have the same charge, there is then no distortion and no variation in mean scattering power amongst the three sites. The presence of the mirror plane characteristic of $C2/m$ in the a and a_r data confirms that M(2) and M(3) are not differentiated in the biotite.

Finally, we consider the titanium data for the biotite. The difference between the patterns for Ti 2*p* and Mg,Fe in the 25—55° region reported previously[7] for a pseudo-*b* rotation is again obvious in the b' and b'' data sets. It had been suggested[7] that the large photoelectron wavelength difference between Ti 2*p* (λ = 0.44 Å) and Mg 2*s*,2*p* or Fe 3*p* (λ = 0.36 Å) was not the cause of this difference. However, throughout the present data, Fe 2*p*, at even longer wavelength (0.54 Å), was also recorded, and the Fe 2*p* patterns show the same effect, a marked change in the intensities of the features in the 40—55° region of the x.p.d. pattern relative to Si, even more clearly. The major part of this difference should thus be attributed simply to wavelength effects.

However, there is one major feature of the new titanium data not common to any of the other octahedral ion data: the large difference between the two sets of pseudo-*a* data [compare Figure 4(*i*) and (*ii*), (*d*) and (*f*), and Figure 5(*i*) (*a*) with (*ii*) (*a*)]. Within each pair of pseudo-*a* axes, the *trans* site remains unaffected by the change of axis whereas the two *cis* sites are interchanged. Because throughout the *a* group of rotations the octahedral ion patterns are made up of different contributions from each of the three sites, this large difference, unique to Ti, shows that Ti must be segregated *either* in the two *cis* sites equally *or* in the *trans* site. Either possibility preserves the mirror plane, so that the good agreement between the titanium data for a and a_r [Figure 3(*ii*) (*a*)] is expected. However, the differences between the curves for Fe, Mg, and Ti here (Figure 3) are not great, suggesting that the Ti has two sites (*i.e.* the *cis* sites) in common with Fe and Mg rather than just one.

To confirm this hypothesis, we compare the profiles of relevant x.p.d. curves with those for lepidolite. Because the ordering pattern there is different, with Li and Mn occupying both *cis* and *trans* sites, unambiguous comparisons can only be made with the b and b_r rotations, in which (uniquely) the two *cis* sites are x.p.d.-equivalent. In these orientations, parallels should exist between the *cis* Al in the lepidolite and any *cis*-segregating ion in the biotite. The most characteristic feature of *cis* Al for the b rotation is that its peak intensity is markedly lower at 12° than is that for Mn,Li [Figure 13(*i*), (*e*), *cf.* (*d*)], leading to a much larger peak in the Si/Al ratio than in Si/Mn,Li at this angle [Figure 12 (*i*), (*c*), *cf.* (*d*)]. Comparison with Figures 6 and 7 shows that this is also a feature of the titanium data in relation to Fe and Mg. Similarly, for the b_r rotation, a major characteristic of Al in lepidolite is a large peak at 53° resulting in a broad minimum in the Si/Al ratio at this angle (Figures 14 and 15). This feature, too, is paralleled in the titanium data (Figures 6 and 7). The effects are less pronounced for Ti because of the low k.e. of Ti 2*p* in comparison with Al 2*s* and 2*p* (*cf.* K and Rb, discussed earlier, for which the k.e. difference is smaller).

We conclude that Ti is indeed segregated in the *cis* sites of the biotite; at such a low concentration (1.2%) this would be impossible to demonstrate with other techniques.

Conclusions

Improved data-collection and analysis techniques, enabling the angular variations of individual x.p.s. peak intensities from complex solids to be separated from the instrument response function, have enabled a significant advance in understanding in detail the origin of the characteristic x.p.d. patterns obtained from the micas. The existence of relatively long-range effects (> 11—13 Å) has been demonstrated unambiguously for the first time, but most features of the data clearly result from short-range interactions.

The value of x.p.d. methods for the detection and characterisation of cation ordering in 1M micas has also been demonstrated. Study of just the two possible rotations (a and a_r) about an axis parallel to the a unit-cell vector rapidly enables differentiation of octahedral M(2) from M(3) to be detected, and should also reveal any long-range tetrahedral ordering. Both these phenomena involve a reduction in symmetry from $C2/m$ to $C2$ and are thus relatively difficult to investigate by conventional crystallography. Comparison of x.p.d. patterns for rotation about the three *b*-group axes at 120° enables ordering within the three octahedral cation sites to be characterised. Rotation about the pseudo-*a* axes is helpful when cations segregate equally in the two *cis* octahedral sites. X.p.d. methods, unlike conventional crystallography, can be applied to cations present in concentrations as low as 1%.

In the 1M lepidolite previously studied by x.p.d.,[6] the M(1), M(2), and M(3) sites are all differentiated. Lithium and Mn occupy the M(1) *trans* site while Al is concentrated in the *cis* M(3) site, as in several other recently studied trioctahedral micas.[27—29] The 1.2% of octahedral Ti in the previously studied[7] 1M biotite is shown to be segregated into the two equivalent *cis* sites, whereas Fe and Mg are essentially randomly distributed amongst the three octahedral sites. Long-range tetrahedral ordering does not occur in either mica.

Acknowledgements

We thank the S.E.R.C. for support, and Drs. J. M. Adams, J. M. Maud, and D. E. Parry for valuable discussions.

References

1 K. Siegbahn, U. Gelius, H. Siegbahn, and E. Olson, *Phys. Lett. A*, 1970, **32**, 221; *Phys. Scr.*, 1970, **1**, 272; C. S. Fadley and S. Å. L. Bergström, *Phys. Lett. A*, 1971, **35**, 375.

2 C. S. Fadley, *Appl. Surf. Sci.*, 1985, **22**, 193.

3 J. M. Adams, S. Evans, P. I. Reid, J. M. Thomas, and M. J. Walters, *Anal. Chem.*, 1977, **49**, 2001.

4 S. Evans, J. M. Adams, and J. M. Thomas, *Philos. Trans. R. Soc. London, Ser. A*, 1979, **292**, 563.

5 L. A. Ash and S. Evans, unpublished work; presented at the RSC Polar Solids Group Meeting, 15th December, 1986.

6 S. Evans and E. Raftery, *Clay Miner.*, 1982, **17**, 443.

7 S. Evans and E. Raftery, *Clay Miner.*, 1980, **15**, 209.

8 S. Evans and E. Raftery, *J. Chem. Res.*, 1982, (*S*) 170.

9 C. S. Fadley, *Prog. Solid State Chem.*, 1976, **11**, 265; C. S. Fadley, in 'Progress in Surface Science,' ed. S. G. Davison, Pergamon, New York, 1984, vol. 16, p. 275.

10 S. Evans and E. Raftery, *Solid State Commun.*, 1980, **33**, 1213.

11 D. E. Parry, paper presented at the Quantum Theory Conference, University of Exeter, September 1986.

12 S. M. Goldberg, R. J. Baird, S. Kono, N. F. T. Hall, and C. S. Fadley, *J. Electron Spectrosc. Relat. Phenom.*, 1980, **21**, 1.

13 W.F. Egelhoff, *Phys. Rev. B*, 1984, **30**, 1052; R. A. Armstrong and W. F. Egelhoff, *Surf. Sci.*, 1985, **154**, L225; E. L. Bullock and C. S. Fadley, *Phys. Rev. B*, 1985, **31**, 1212.

14 S. Evans, R. G. Pritchard, and J. M. Thomas, *J. Phys. C*, 1977, **10**, 2483.

15 P. A. Lee, P. H. Citrin, P. Eisenberger, and B. M. Kincaid, *Rev. Mod. Phys.*, 1981, **53**, 769.

16 D. E. Parry, unpublished work.

17 See, for example, S. W. Bailey, in 'Crystal Structures of Clay Minerals and their *X*-Ray Identification,' eds. G. W. Brindley and G. Brown, Mineralogical Society, London, 1980, p. 1.

18 A. Baronnet, in 'Current Topics in Materials Science,' ed. E. Kaldis, North-Holland, Amsterdam, 1980, vol. 5, p. 447.

19 D. T. Clark and D. Shuttleworth, *J. Electron Spectrosc. Relat. Phenom.*, 1979, **17**, 15.

20 S. Evans and D. A. Elliott, *Surf. Interface Anal.*, 1982, **4**, 267.

21 S. Evans and C. E. Riley, *J. Chem. Soc., Faraday Trans. 2*, 1986, 541.

22 S. Evans, *Proc. R. Soc. London, Ser. A*, 1978, **360**, 427.

23 J. M. Adams, S. Evans, and J. M. Thomas, *J. Phys. C*, 1973, **6**, L382.

24 S. Evans and A. G. Hiorns, *Surf. Interface Anal.*, 1986, **8**, 71.

25 D. A. Shirley, *Phys. Rev. B*, 1972, **5**, 4709.

26 A. Savitsky and M. J. E. Golay, *Anal. Chem.*, 1964, **36**, 1627.

27 S. Guggenheim, *Am. Mineral.*, 1981, **66**, 1221.

28 S. W. Bailey, in 'Reviews in Mineralogy,' ed. S. W. Bailey, Mineralogical Society of America, Washington D. C., 1984, vol. 13, p. 13.

29 S. W. Bailey, *Clays Clay Miner.*, 1984, **32**, 81.

30 See, for example, W. Joswig, H. Fuess, R. Rothbauer, Y. Takeuchi, and S. A. Mason, *Am. Mineral.*, 1980, **65**, 349.

31 J. G. Thompson, Ph.D. Thesis, James Cook University of North Queensland, Australia, 1985.

32 J. G. Thompson, *Clay Miner.*, 1984, **19**, 229.

33 C. P. Herrero, J. Sanz, and J. M. Serratosa, *Solid State Commun.*, 1985, **53**, 151.

34 J. Sanz and J. M. Serratosa, *J. Am. Chem. Soc.*, 1984, **106**, 4790.

35 N. C. M. Alma, G. R. Hays, A. V. Samoson, and E. T. Lippmaa, *Anal. Chem.*, 1984, **56**, 729.

36 M. Lipsicas, R. H. Raythatha, T. J. Pinnavaia, I. D. Johnson, R. F. Giese, P. M. Costanzo, and J-L. Robert, *Nature* (*London*), 1984, **309**, 604.

37 E. S. Crawford, S. Evans, E. Raftery, and M. D. Scott, *Surf. Interface Anal.*, 1983, **5**, 28.

Received 2*nd July* 1987; *Paper* 7/660